Composite Structures 331 (2024) 117864

Contents lists available at ScienceDirect

Composite Structures

journal homepage: www.elsevier.com/locate/compstruct

Confinement of masonry with FRCM composites: Strength predictive models

Annalisa Napoli *, Roberto Realfonzo

Department of Civil Engineering, University of Salerno, Via Giovanni Paolo II, 132, 84084 Fisciano, SA, Italy

ARTICLE INFO

Keywords:
Masonry
Confinement
Fabric reinforced cementitious matrix (FRCM)
Strength models

ABSTRACT

Fabric reinforced cementitious matrix (FRCM) composites have emerged as an appealing alternative to fiber reinforced polymer (FRP) for the external confinement of masonry members; nevertheless, their use in practice is limited due to the lack of reliable formulas to estimate the compressive strength and ultimate strain of confined members.

By following a recently published study, new formulas for the prediction of the compressive strength of the FRCM confined masonry are proposed here, which were obtained by considering an updated experimental database compiled from the literature.

These formulas were developed by applying error minimization techniques to the collected experimental results; test data were treated in different ways, such as: (*a*) separating the members made of natural stones from those built with artificial blocks, and (*b*) treating separately the fiber types (basalt, carbon, glass, PBO and steel) of the FRCM system, or (*c*) considering the experimental data all together.

Finally, to evaluate the reliability of the developed relationships, the strength predictions provided by the new proposals were compared with those obtained using the expressions reported in some international guidelines.

1. Introduction

Fabric reinforced cementitious matrix (FRCM) composites are obtained by embedding an open grid fabric made of continuous fibers in different types of matrices (e.g. lime-based mortar, cement-based mortar, and geopolymers). Obviously, various combinations of fibers and matrices, as well as different percentages of fibers, lead to different physical and mechanical properties of the composite.

The most commonly fibers used in FRCM composites are: basalt (B), carbon (C), glass (G) and poliparafenilenbenzobisoxazole (PBO). These fibers are typically arranged in bundles which are opportunely spaced to facilitate their impregnation and assure matrix continuity among internal and external matrix layers. Unidirectional steel (S) textiles composed of properly spaced ultra-high tensile strength steel cords of twisted micro-wires are also frequently considered for applications with inorganic matrix; such composites are termed steel fabric reinforced cementitious mortar (S-FRCM) or steel fiber reinforced grout (SRG) [1,2].

Lately, the use of inorganic matrix in combination with natural fibers (such as, flax, hemp, sisal or jute) has also attracted the interest of the scientific community in the objective of addressing several issues in the construction industry related to sustainability [3-6].

With respect to fiber reinforced polymers (FRPs), the application of FRCM composites to masonry members is preferable due to several reasons, among which: better composite-substrate compatibility, higher permeability of the strengthened surface and reduced invasiveness of the retrofitting technique coupled with satisfactory levels of reversibility (or at least removability) [7-11].

Because of the relatively more recent commercialization, the experimental studies concerning concrete or masonry members reinforced with FRCM systems are less numerous than those regarding members retrofitted by FRP ones. However, the experimental results obtained so far have generally shown the effectiveness of using the FRCM composites to increase both the in-plane and out-of-plane capacity of masonry walls [12-16], the collapse loads of masonry arches [17,18] and the compressive strength of masonry columns for which an overview of the experimental and theoretical research has been recently reported in [19]. Concerning the more recent introduction of FRCM composites with respect to FRPs, it is worth highlighting that, for masonry confinement, the pioneer experimental investigations date from 2015 only [20-22].

* Corresponding author.
E-mail addresses: annapoli@unisa.it (A. Napoli), rrealfonzo@unisa.it (R. Realfonzo).

https://doi.org/10.1016/j.compstruct.2023.117864
Received 1 June 2023; Received in revised form 20 November 2023; Accepted 28 December 2023
Available online 2 January 2024

Nomenclature

The following symbols are used in this paper:

B	=width of square or rectangular cross section
BD	=bidirectional strengthening sheet
D	=diameter of circular cross section
DB	=debonding of the reinforcement at the overlap region
E_f	=elastic modulus of dry strengthening sheet
E_i	=*i*-th error calculated according to MAPE error
E_{mat}	=elastic modulus in compression of FRCM matrix
$(E_{rr})_m^{MAPE}$	=mean absolute percentage error
FM	=dominant failure mode exhibited by test specimens
$f_{mat,b}$	=flexural strength of FRCM matrix
$f_{mat,c}$	=compressive strength of FRCM matrix
$f_{f,u}$	=ultimate tensile strength of dry strengthening sheet
f_l	=lateral confining pressure of FRCM confinement
$f_{l,eff}$	=effective lateral confining pressure of FRCM confinement
$\bar{f}_{l,eff}$	=normalized effective lateral confining pressure, i.e.: $\frac{f_{l,eff}}{f_m}$
f_m	=compressive strength of unconfined masonry
$\bar{f}_{mc}^{\ exp}$	=experimental value of normalized compressive strength of FRCM confined masonry
$\bar{f}_{mc}^{\ th}$	=theoretical value of normalized compressive strength of FRCM confined masonry
$\bar{f}_{mc,i}^{\ exp}$	=*i*-th experimental value of normalized compressive strength of FRCM confined masonry
$\bar{f}_{mc,i}^{\ th}$	=*i*-th theorethical value of normalized compressive strength of FRCM confined masonry
H	=depth of square/rectangular cross-section
g_m	=masonry mass density
JF	=FRCM jacket failure
k_{eff}	=FRCM confinement efficiency coefficient
k_H	=coefficient of horizontal efficiency of FRCM confinement
k_{mat}	=coefficient of FRCM confinement efficiency related to the presence of inorganic matrix
k_V	=coefficient of efficiency of FRCM confinement
k_ε	=strain efficiency factor of the FRCM system
L	=height of specimen
L_b	=overlapping length of the FRCM
N	=number of specimens
n	=number of datasets
n_f	=number of FRCM layers
p'_f	clear distance between FRCM strips in case of discontinuous wrapping
r_c	=corner radius
S	=fiber–matrix slippage
t_f	=total thickness of the employed fiber reinforcement, i.e.: $t_f = n_f\ t_{f,j}$
$t_{f,j}$	=equivalent thickness of the single layer of the fiber sheet
t_{mat}	=overall thickness of the FRCM matrix
UD	=unidirectional strengthening sheet
$\alpha_1, \alpha_2, \cdots, \alpha_5$	=fine-tuning models coefficients
γ_f	=density of strengthening sheet
$\varepsilon_{f,u}$	=ultimate strain of dry strengthening sheet
$\varepsilon_{j,u}$	=ultimate hoop strain experimentally measured in FRCM jacket
ρ_{mat}	=matrix reinforcement ratio

A first state of the art on the FRCM strengthening of masonry structures was published in 2018 [23], followed by a more recent review authored by Irandegani et al. [24] and other overviews limited to the use of S-FRCM systems [25,26].

Simultaneously with investigating the efficiency of the FRCM systems in improving the behavior of masonry members, a great effort was carried out by some researchers to characterize the tensile behaviour of these composites and their adhesion to different masonry substrates with the purpose to publish preliminary recommendations [27,28].

Despite the limited amount of data and information available for the development of reliable design formulae, accredited guidelines for the strengthening of structural members with FRCMs are now available, such as the Italian guide CNR-DT 215 [29], applicable to both concrete and masonry structures, and the even more recent American guide ACI 549.6R [30] specifically edited for repair and strengthening of masonry.

However, despite the significant advances of the knowledge made in addressing the key aspects related to the FRCM masonry strengthening, there is still a lot of work to do in collecting and analyzing all the available information as well as in validating and/or improving the reliability of the analytical formulations proposed in international guidelines.

To this purpose, the compressive behavior of FRCM confined masonry columns is one of the most debated topics. To date, indeed, the knowledge on the subject is rather poor [21-31], and fragmented, and sometimes controversial; therefore, the development of reliable relationships for the estimate of the compressive strength and ultimate strain of the FRCM confined masonry is a challenging task.

Concerning the fragmentation of information it is worth highlighting that, when a large number of tests could not be carried out, researchers often chose to investigate many study parameters at the same time, such as type of fiber, number of layers, mesh geometry, etc., therefore, losing sight of the real focus of the performed study.

Finally, the information is believed uneven and controversial in the sense that a variety of fabric meshes - composed of an equally higher variety of fibers - were embedded in inorganic matrices characterized by different mechanical properties. As a result, understanding the "weight" of the different parameters in the characterization of the FRCM confinement efficiency is the key for the development of reliable design formulae.

As a natural effect from the general misunderstanding on the topic, most of the collected studies generally focus on investigating the applicability of existing formulations suitable for FRP systems to the case of FRCM ones; a few others provide promising proposals even though they were validated by using a limited number of experimental data.

With the aim to improve the knowledge, a *Round Robin Test* (RRT) program was recently organized within the framework of the "*DPC-ReLUIS 2019–2021 Project*", which was financially supported by the Italian Department of Civil Protection (DPC), and involved numerous universities, and to which the authors of this paper took part.

The obtained results, which are available in a recently published paper [32], helped to gain an insight into the contribution of the FRCM on the axial behavior of confined masonry columns, by varying some parameters, such as: the type of masonry (natural or artificial), the FRCM system (G-FRCM or S-FRCM) and the number of reinforcement layers (one, two or three).

With the purpose to organize all the available information in a systematic framework, in a recent paper the authors published a wide experimental database based on which first analytical proposals for estimating the compressive strength of masonry members confined by FRCM, suitable for both any fiber (B, C, G, PBO, and S) and masonry type (natural and artificial) were proposed [19].

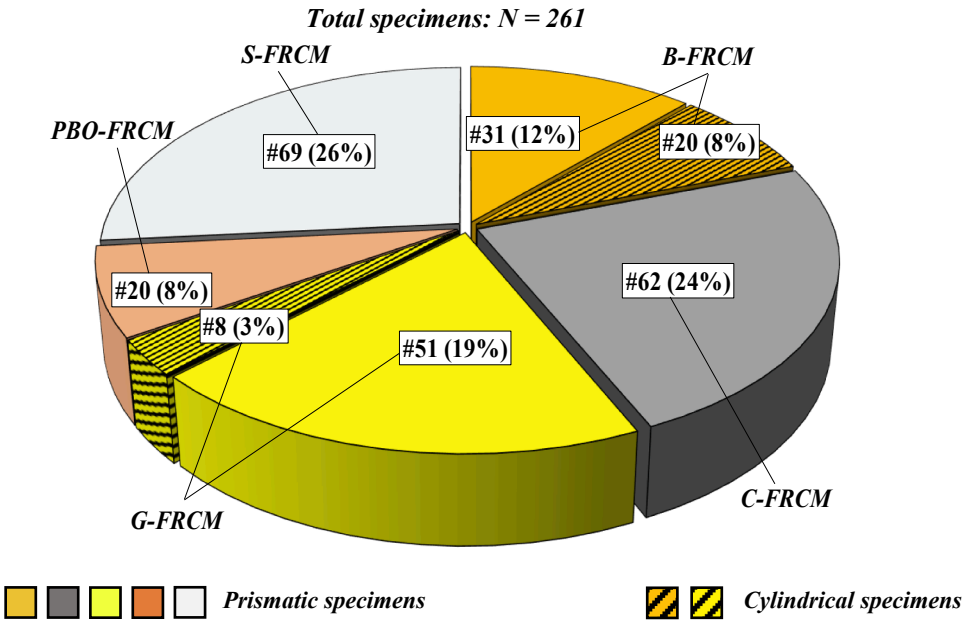

Fig. 1. Distribution of specimens per FRCM system within the database.

By following the study outcomes published in [19], a further contribution to advancing the knowledge on the compressive strength of FRCM confined masonry is provided in this paper, which can also be eventually considered for an integration/upgrading of the existing guidelines CNR-DT 215 [29] and ACI 549.6R [30]. To this purpose, it is worth highlighting that the present study is part of the research activities planned within the ReLUIS-DPC 2022–2024 project (WP14) funded by the Italian Department of Civil Protection (https://www.reluis.it/it/progetti-dpc-reluis/dpc-reluis-2022-2024.html), which objective is to provide research contributes useful for improving the current design guidelines CNR-DT 215 [29]. As such, the authors are involved in the updating of the chapter concerning the FRCM confinement of masonry, with the purpose to investigate the reliability of the formulation currently reported in the document – originally validated on a poor representative experimental database – and its applicability to all the types of FRCM systems covered by the document. This implies that the study focuses on the "most scientifically" investigated FRCM systems, i.e., on the composites employing synthetic fibers like carbon, glass, PBO and steel and on those entailing basalt fibers which are of mineral nature; these are also the fiber types considered in the mentioned documents. Conversely, the most recently explored composites made of plant-based natural fibers (let's say flax, hemp and jute), for which more investigation is needed, are not included in the study.

First, un upgrade of the collected database - the largest to the authors' knowledge – is presented and deeply described here.

Then, refined predictive models for the compressive strength of the FRCM confined masonry were derived by applying best-fit techniques to the experimental results and compared with those previously found by the authors in the case of both FRCM and FRP applications [19,33]. On this aspect, it should be immediately clarified that the collected database highlights a significant scattering of experimental results and therefore, the calibration of models' key parameters based on minimizing the overall error between experiments and predictions could fail in some specific cases. This issue, therefore, has led the authors to select an error minimization technique that, with respect to others, mostly provides conservative predictions.

The accuracy of the analytical proposals is here also examined by considering the typology of masonry, artificial and natural, the latter poorly investigated in the literature. Furthermore, analytical formulations were calibrated by considering each type of FRCM system separately with the purpose to investigate, based on the collected data, that providing the "best" performance in terms of increase of compressive strength. Even though further validation of the proposed relationships will be needed, the present study highlights the improved accuracy of the proposed models with respect to the companion formulations reported in the mentioned guidelines CNR-DT 215 (2018) [29] and ACI 549.6R (2020) [30]; some criticisms related to the expressions reported in these documents are also highlighted.

2. Database update

As already mentioned, the database presented in [19] has been recently updated by including other data and results of uniaxial compression tests performed on masonry members confined by FRCM systems. In particular, the current number (N) of specimens is 261 (against 222 indicated in the previous database), of which 28 with circular cross-section and investigated only in the case of B- and G-FRCM systems.

The addition of new data has basically expanded the data sample previously available for PBO-FRCM (from 14 to 20 samples) and S-FRCM systems (from 53 to 69 members) applied to square/rectangular specimens.

The pie chart in Fig. 1 shows the current distribution of specimens in the database per FRCM system. Regardless of the shape of the cross-section, the collected specimens are rather equally distributed among the examined FRCM systems, except for the PBO-FRCM for which only 20 specimens are available. Specifically, the database includes:

– 51 specimens confined with B-FRCM (31 prismatic and 20 cylindrical);

– 62 specimens confined with C-FRCM (only prismatic);

– 59 specimens confined with G-FRCM (51 prismatic and 8 cylindrical);

– 20 specimens confined with PBO-FRCM (only prismatic);

– 69 specimens confined with S-FRCM (only prismatic).

All specimens were confined by using a continuous wrapping and employing a variable number of layers. An exception is represented by three tests relative to PBO-FRCM confinement for which a discontinuous wrapping was used [34].

The main details related to tests collected for the analytical study are summarized in Table A.1 and Table A.2 (see Appendix A) for the case of

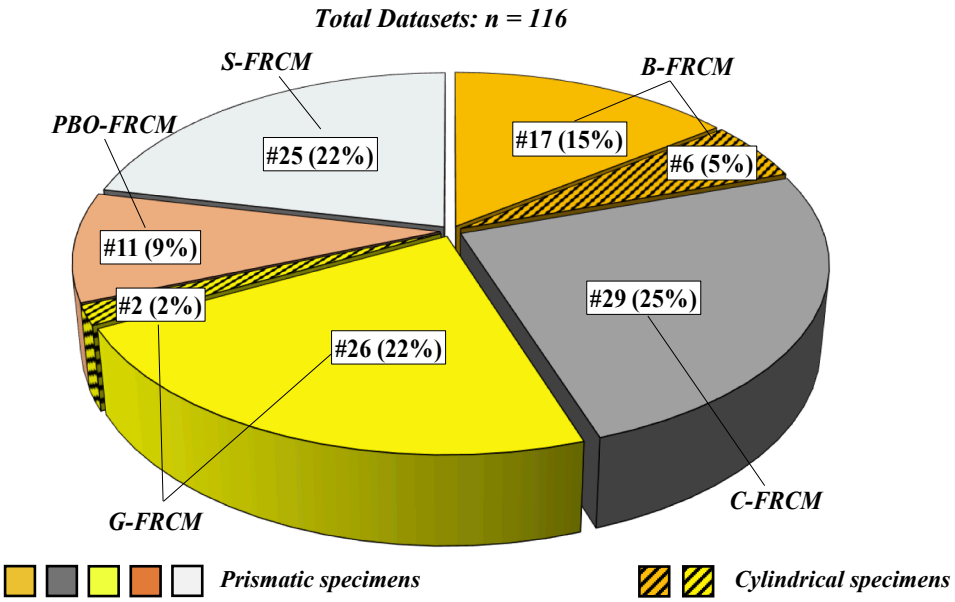

Fig. 2. Distribution of datasets per FRCM system.

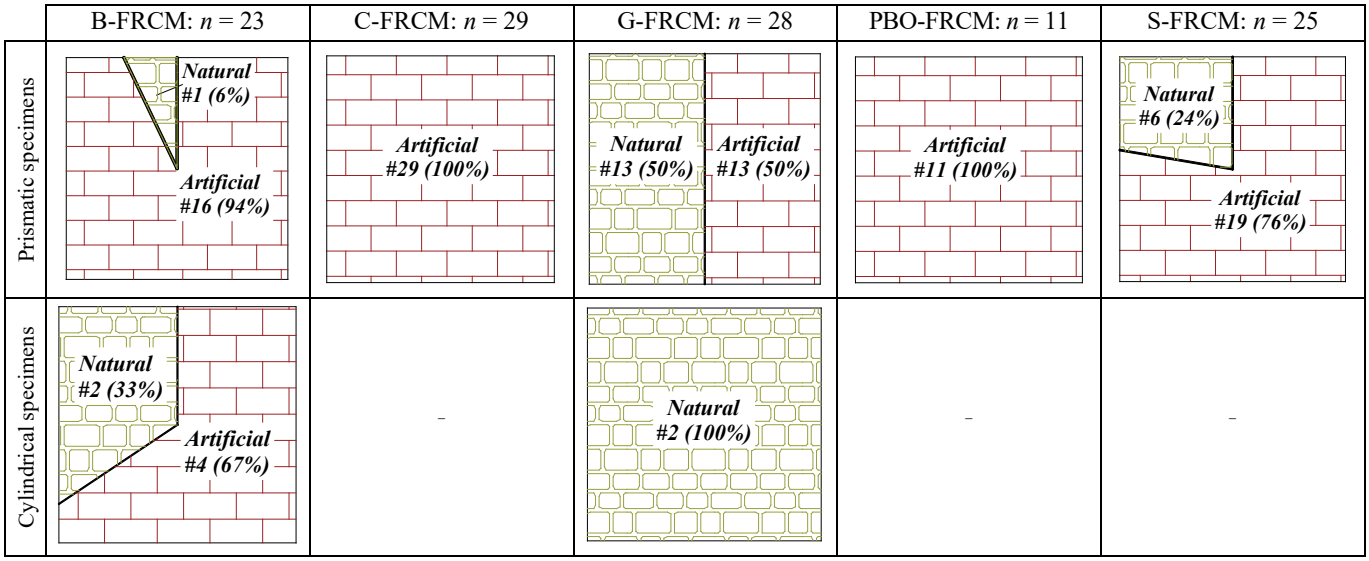

Fig. 3. Distribution of datasets per masonry type within each FRCM confining system.

prismatic and cylindrical specimens, respectively. It is worth highlighting that the information reported in these tables is not referred to the 261 tests collected in the general database, but it is directly reorganized in 116 homogeneous datasets, of which 108 referred to prismatic specimens (corresponding to 233 members of the general database) and only 8 to cylindrical ones (corresponding to 28 members of the general database).

The organization in datasets is consistent with the methodology followed in the previous investigations [19–33,50–53] which is in turn based on the "Design by testing" approach recommended by the Annex D of Eurocode 0 [54].

The pie chart in Fig. 2 shows the distribution of the 116 datasets per FRCM system.

The 51 compression tests performed using prismatic (#31) and cylindrical (#20) samples confined with B-FRCM system, were grouped in 17 and 6 datasets, respectively, covering about 20% of the database (n = 23 datasets). The 62 test results on specimens confined with C-FRCM systems, instead, were reorganized in 29 datasets (exactly a quarter of the database). Moreover, the experimental test results concerning the 59 specimens confined with G-FRCM systems (51 prismatic plus 8 cylindrical) were grouped in 28 datasets, covering 24% of the database, of which 26 refers to prismatic members and 2 to cylindrical ones. Finally, results from 20 tests conducted on PBO-FRCM confined samples were converted into 11 datasets (only 9.5% of the database), and the 69 test results on members confined by S-FRCM systems were grouped in 25 datasets, corresponding to 21.5% of the database.

For each considered FRCM confinement system, the information on the type of bricks (artificial) and blocks (natural) of which the masonry columns' datasets were made is noteworthy. To this purpose, Fig. 3 shows the per cent distribution of the datasets per masonry type. It can be observed that artificial masonry (AM) columns made of clay bricks (CBs) are the most studied (92 datasets out of a total 116, i.e. about 80%): in particular, all the samples confined with C- and PBO-FRCM systems were made of this kind of masonry.

The six datasets including samples confined by S-FRCM systems and consisting of natural blocks were made using tuff units (TUs), a type of

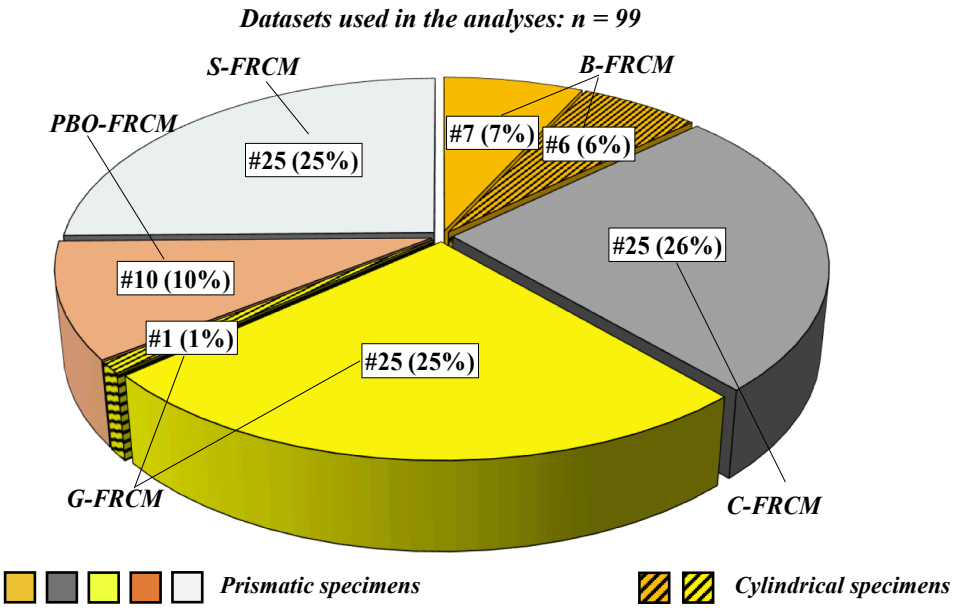

Fig. 4. Distribution of datasets used in the analyses per FRCM system.

natural masonry (NM) widely used in Southern Italy in the past for the construction of buildings.

In the case of columns confined by G-FRCM jackets, most of the datasets concern tests carried out on samples made with natural blocks: in the case of prismatic columns, 6 datasets concern samples made of TUs, 4 datasets samples built with limestone blocks (LS) and 3 datasets specimens made of calcarenite (CALC), a sort of limestone composed by sand and carbonate grains, very common in several regions in the Mediterranean area. The remaining two datasets concern cylindrical columns made of calcarenite.

Finally, only 3 datasets concern compression tests performed on NM columns confined with B-FRCM jackets: these tests were conducted on prismatic (#1 dataset) and cylindrical (#2) samples made using LS and CALC blocks.

In order to perform the analyses described in the next section, the number n of datasets was reduced from 116 to 99 due to some issues related to either missing values for some key parameters or questionable test results deserving more investigation. The datasets reduction involved all the types of confining FRCM systems, with the sole exception of the S-FRCM one.

In particular, it has not been possible to include datasets in the analyses when: a) the ultimate strain of the fiber mesh ($\varepsilon_{f,u}$) was lacked; b) the value ($\bar{f}_{mc}$) of the ratio between the compressive strength of the confined masonry (f_{mc}) and that of the unconfined masonry (f_m) was less than or at most equal to 1. On this last aspect, indeed, it is quite trivial to expect that, when the FRCM confining action is ineffective, the compressive strength of the confined masonry f_{mc} approximately coincides with the performance of the unconfined member. Cases of confinement inefficacy will deserve more investigation and may be due to several reasons, among which the non-perfect application of the FRCM system.

Therefore, the pie chart in Fig. 4 shows the distribution per FRCM system of the 99 datasets effectively used in the analyses.

These datasets involve 227 specimens (against the 261 originally collected). The most significant reduction has regarded the B-FRCM system (10 datasets removed) whose data were finally grouped in 13

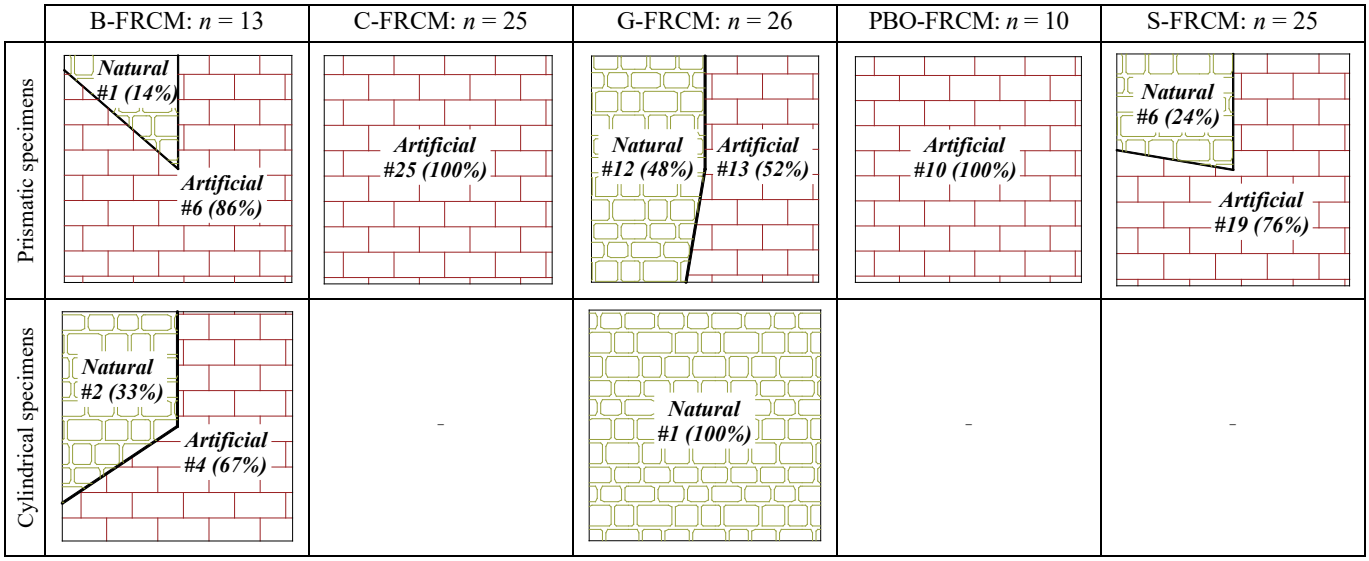

Fig. 5. Distribution of datasets used in the analyses per masonry type within each FRCM confining system.

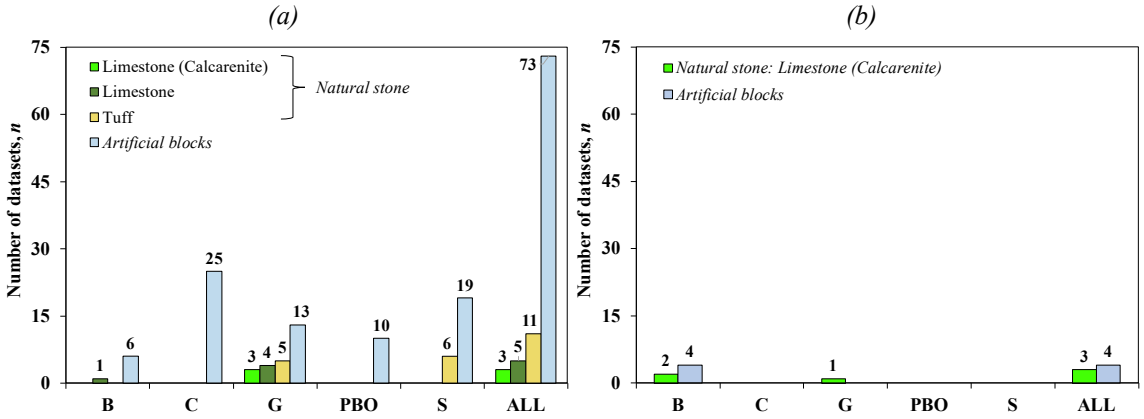

Fig. 6. Masonry types identified in the datasets used in the analyses and their distribution per FRCM system: (a) prismatic columns; and (b) cylindrical columns.

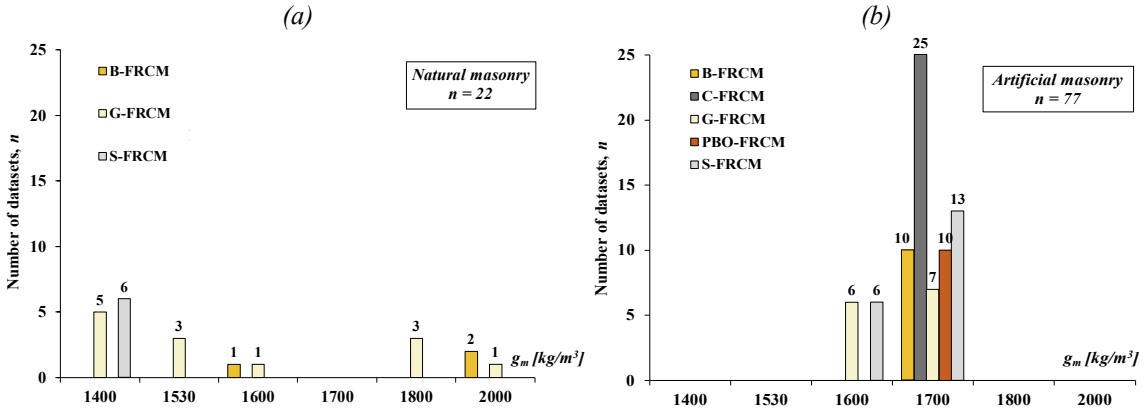

Fig. 7. Distribution of datasets per masonry mass density within the FRCM systems: (a) prismatic specimens; and (b) cylindrical specimens.

datasets (7 related to prismatic specimens and 6 to cylindrical one) including a total of 37 specimens (17 prismatic and 20 cylindrical), which cover the 13% of the "new" database. For the C-FRCM system, instead, the remaining datasets are 25, covering about 26% of the database and collecting a total of 50 prismatic specimens; for the G-FRCM system, the valid datasets are 26 (25 prismatic + 1 cylindrical), covering the 26% of the database and collecting 53 specimens (49 prismatic and 4 cylindrical); in the case of PBO-FRCM, the datasets useful for the analyses are 10, covering the 10% of the database and collecting 10 prismatic columns; finally, in the case of the S–FRCM system the number of datasets does not change, so those useful to the analyses are 25, covering the 25% of the database and involving all the specimens originally collected (N = 69).

For all the FRCM confining systems, Fig. 5 shows the updated number of datasets per each of the two categories of masonry (natural and artificial).

Comparing Fig. 5 with Fig. 3 the following observations can be made:

- Similarly to the C- and PBO- FRCM systems - with 4 and 1 datasets removed, respectively - the 10 datasets discarded in the case of the B-FRCM system exclusively regard AM's columns (i.e. masonry samples made of clay bricks);
- conversely, in the case of the G-FRCM system, the 2 datasets excluded from the analyses are relative to tests performed on prismatic columns made of tuff units and on cylindrical ones made of calcarenite, respectively;

Finally, the bar charts in Fig. 6a and 6b specify, within each masonry type, the number of datasets involved in the case of prismatic and cylindrical specimens, respectively.

By better analyzing the database in Tables A.1 and A.2, noteworthy is the information about the masonry mass density g_m which is a parameter believed affecting the FRCM performance.

To this purpose, indeed, the nonlinear strength model suggested by DT 215 [29] - similarly to what already done in the document DT 200 R1 [55] for FRP confinement applications - accounts for the contribution of the masonry mass density g_m (expressed in kg/m^3) in the estimate of f_{mc}; specifically, this parameter roughly considers the influence of voids and porosity of both the constituent materials and the masonry texture itself on the estimated axial strength [56]. However, looking at the 99 datasets considered for the analyses, it can be observed that the value of g_m is always provided in the scientific papers when it is referred to the natural masonry, while in the case of CB this information is often omitted and, therefore, an average value of g_m equal to 1700 kg/m^3 is assumed by the authors and considered in the analyses.

The bar charts in Fig. 7 show the number of datasets per g_m value within each FRCM system in the case of both NM (Fig. 7a) and AM (Fig. 7b). In the case of NM, most datasets have g_m values lower than 1600 kg/m^3, with the highest concentration about 1400 kg/m^3; in the case of CB, instead, it is trivial to observe that the datasets are mostly concentrated about the value of 1700 kg/m^3 set by the authors, since only for a dataset related to the C-FRCM system [22,41] and for another one related to the G-FRCM system [41] the scientific papers specifically provide g_m = 1700 kg/m^3. This consideration will be useful for the analytical study presented in the next section.

Another examined parameter is the ratio between the compressive strength of the mortar employed for the FRCM system and the compressive strength of the unconfined masonry $\frac{f_{mat,c}}{f_m}$.

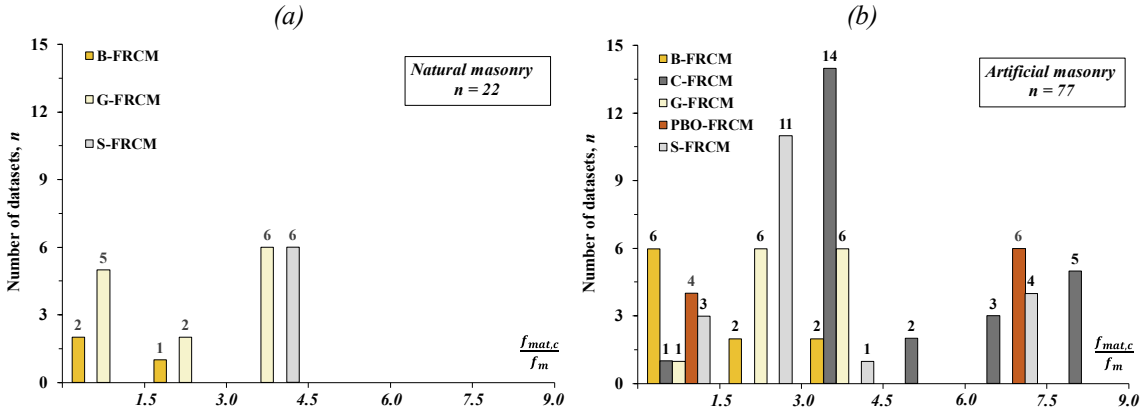

Fig. 8. Distribution of datasets based on the ratio between the compressive strength of the confined masonry and the compressive strength of the unconfined masonry ($\frac{f_{mat,c}}{f_m}$): (a) natural masonry; and (b) artificial masonry.

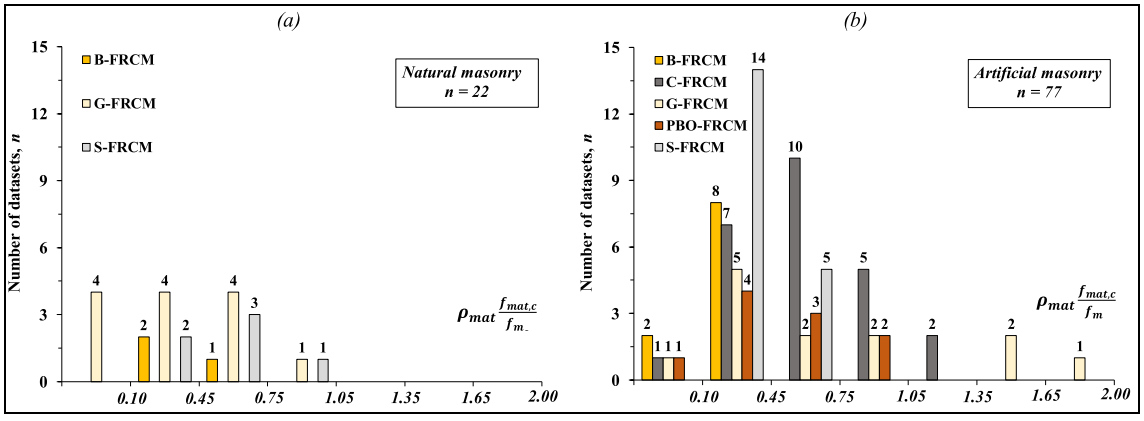

Fig. 9. Distribution of datasets based on the parameter $\rho_{mat}\ \frac{f_{mat,c}}{f_m}$: (a) prismatic specimens; and (b) cylindrical specimens.

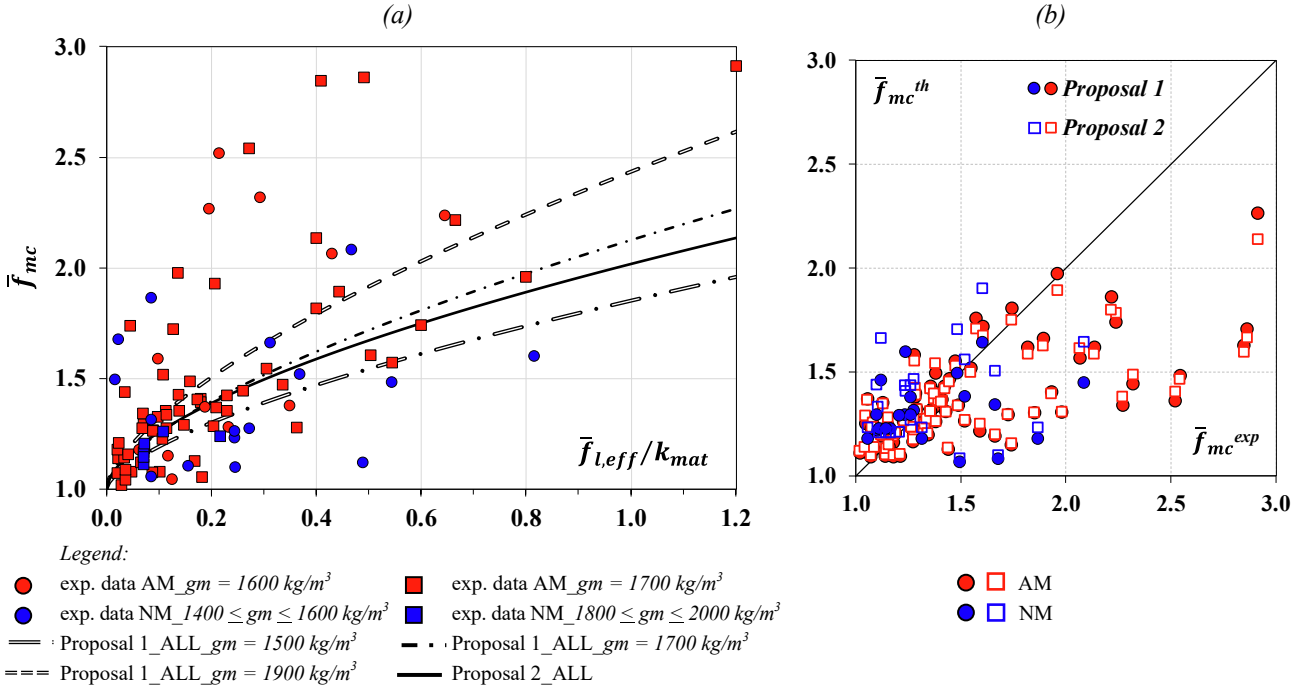

Fig. 10. *Proposal 1* and *2* obtained by considering all datasets (a), and comparison between experimental data and predictions (b).

According to the current version of DT 215 [29], this ratio has some relevance since it enters the estimate of k_{mat} which is the parameter accounting for the contribution of the inorganic matrix and affecting the estimate of the lateral confining pressure. This parameter is given by:

$$k_{mat} = 1.81 \left(\rho_{mat} \frac{f_{mat,c}}{f_m}\right)^2 \leq 1 \quad (1)$$

where ρ_{mat} is the matrix reinforcement ratio expressed by:

$$\rho_{mat} = 4 \frac{t_{mat}}{D} \leq 1 \quad (2)$$

In Eq. (2), t_{mat} is the total thickness of the FRCM matrix, while D is the diameter of the circular cross-section or the diagonal length of the square or rectangular cross-section.

To this purpose, the bar charts in Fig. 8 show the distribution of datasets for the case of NM (Fig. 8a) and AM (Fig. 8b). As shown, the datasets are rather scattered, covering a wide range of values from lower than 1.5 up to lower than 9. In the case of NM, the values are mostly distributed in the left side of the graph with the highest concentration in the range [3.0–4.5]. In the case of AM, the slightly highest concentration is again in the range [3.0–4.5] but a good number of datasets also falls in field of $\frac{f_{mat,c}}{f_m}$ lower than 3 and higher than 6.

By focusing on Eq. (1), the last parameter under consideration is straightly the product $\left(\rho_{mat} \frac{f_{mat,c}}{f_m}\right)$, and Fig. 9 shows the distribution of datasets based on specific ranges of values for the case of NM (Fig. 9a) and AM (Fig. 9b). Whatever the FRCM system and the masonry type, most datasets are concentrated in the wide range [0.10–0.75]. Conversely, by focusing on the fiber type, the datasets are rather scattered since they cover almost all the considered ranges; this observation is particular evident in the case of the G-FRCM system applied to artificial masonry, showing datasets also falling in the range with $\left(\rho_{mat} \frac{f_{mat,c}}{f_m}\right) > 1.35$, and in the case of C-FRCM system, with datasets covering a wide range $0 < \left(\rho_{mat} \frac{f_{mat,c}}{f_m}\right) \leq 1.35$.

Of course, it is worth highlighting that, in order develop a reliable strength model, the variability of several geometric and mechanical parameters should be examined, in addition to those reported in the above Figs. 7-10, such as: the variability of both the cross-section dimension and height of members, the different geometry of the strengthening sheet and the mechanical characteristics of the FRCM matrix (some of these parameters are investigated in Appendix A). However, based on the available data, it is very hard to quantify their specific influence on the strength performance if the other parameters are not taken constant. Hopefully, with the increase of the of the experimental database in future, this aspect will be better investigated.

3. The analytical study

In the present study, new analytical formulas for the estimate of the compressive strength of masonry confined by FRCM (f_{mc}), were developed through best-fit analyses applied to the 99 experimental datasets. The general five-parameter relationship described by Eqs. (3) was considered which is derived from the relationship reported in the CNR-DT 215 [29], i.e.:

$$\bar{f}_{mc} = \frac{f_{mc}}{f_m} = 1 + \alpha_2 \left(\frac{g_m}{1000}\right)^{\alpha_3} \bar{f}_{l,eff}^{\ \alpha_1} = 1 + \alpha_2 \left(\frac{g_m}{1000}\right)^{\alpha_3} \left(k_H k_V \frac{\frac{1}{2}\rho_f E_f k_{mat} \varepsilon_{f,u}}{f_m}\right)^{\alpha_1} \quad (3)$$

where:

- $\bar{f}_{mc}$ is the compressive strength of the FRCM confined masonry f_{mc} normalized with respect to the compressive strength of the unconfined masonry f_m, and.

- $\bar{f}_{l,eff} = \frac{f_{l,eff}}{f_m}$ is the effective lateral confining pressure exerted by the FRCM normalized to f_m, being $f_{l,eff}$ given by:

$$f_{l,eff} = k_{eff} \ f_l = k_H \ k_V \ \frac{1}{2} \ \rho_f \ E_f \ k_{mat} \ \varepsilon_{f,u} \quad (4)$$

where $k_{eff} = k_H \ k_V \leq 1$ is the parameter accounting for the shape of the section and the type of FRCM wrapping (continuous or discontinuous), in which the coefficient of horizontal efficiency k_H is calculated according to the guidelines DT 215 [29] and the coefficient of vertical efficiency k_V is estimated as suggested by DT 200 R1 [55].

In Eq. (4):

- $\rho_f = 4 \ t_f/D$ is the geometric strengthening ratio related to the FRCM system, being tf the total thickness of the employed strengthening sheet, and D the diameter of the circular cross-section or the diagonal length of the square or rectangular cross-section;

- k_{mat} is the dimensionless coefficient of confinement efficiency accounting for the presence of the inorganic matrix, which has the following more general expression with respect to Eq. (1):

$$k_{mat} = \alpha_4 \left(\rho_{mat} \frac{f_{mat,c}}{f_m}\right)^{\alpha_5} \leq 1 \quad (5)$$

where the matrix reinforcement ratio ρ_{mat} is given by Eq. (2).

Therefore, by introducing the expression for k_{mat} in Eq. (3), the dimensionless compressive strength of a FRCM confined member becomes:

$$\bar{f}_{mc} = \frac{f_{mc}}{f_m} = 1 + \alpha_2 \left(\frac{g_m}{1000}\right)^{\alpha_3} \left[k_H \ k_V \frac{\frac{1}{2} \ \rho_f \ E_f \ \alpha_4 \left(\rho_{mat} \frac{f_{mat,c}}{f_m}\right)^{\alpha_5} \varepsilon_{f,u}}{f_m}\right]^{\alpha_1} \quad (6)$$

where the α_i parameters are the fine-tuning parameters to be calibrated through a proper error minimization technique. In this study, the mean absolute percentage error (MAPE) was selected to minimize the error between experiments and predictions in terms of $\bar{f}_{mc}$; based on previous investigations performed by the authors, this technique yields the most conservative results in terms of model calibration [19,50].

In particular, the overall error estimated according to MAPE $(E_{rr})_m$ on the considered number n of datasets is given by:

$$(E_{rr})_m = \frac{\sum_{i=1}^{n} |E_i|}{n}; E_i = \frac{\left(\bar{f}_{mc,i}^{exp} - \bar{f}_{mc,i}^{th}\right)}{\bar{f}_{mc,i}^{exp}} \ 100 \quad (7)$$

where E_i is the i-th error between experiment $(\bar{f}_{mc,i}^{exp})$ and prediction $(\bar{f}_{mc,i}^{th})$. A few preliminary results can be found in recent paper [57].

Concerning the strength model expressed by Eq. (6), it is worth to highlight that, according to CNR-DT 215 [29], the coefficient α_1 can be assumed equal to 0.5 in absence of reliable experimental results, while

Table 1
Cases of analysis.

Case #	n_α	α_i	α_1	α_2	α_3	α_4	α_5
1	5	$\alpha_1, \alpha_2, \alpha_3, \alpha_4, \alpha_5$					
2	4	$\alpha_1, \alpha_2, \alpha_4, \alpha_5$			0.00		
3	3	$\alpha_1, \alpha_4, \alpha_5$		1.00	0.15		
4		$\alpha_1, \alpha_4, \alpha_5$		1.10	0.00		
5	2	α_4, α_5	0.50	1.00	0.15		
6		α_4, α_5	0.40	1.10	0.00		
7		α_1, α_2			1.00	1.81	2.00
8		α_4, α_5	0.50	1.00	1.00		
9	1	α_5	0.50	1.00	0.15	1.00	
CNR-DT 215 [29]	–	–	0.50	1.00	1.00	1.81	2.00

Table 2
Strength models suitable for: any masonry type, artificial masonry only and natural masonry only.

Masonry	n	*Proposal 1*		*Proposal 2*	
		Describing Equation	$(E_{rr})_m$	Describing Equation	$(E_{rr})_m$
Any (ALL)	99	$\bar{f}_{mc} = 1 + 0.35\left(\frac{g_m}{1000}\right)^{2.20}\bar{f}_{l,eff}^{\,0.65}$ $k_{mat} = 1.00$	13.21%	$\bar{f}_{mc} = 1 + 1.05\,\bar{f}_{l,eff}^{\,0.60}$ $k_{mat} = 0.95$	13.64%
Artificial Masonry (AM)	77	$\bar{f}_{mc} = 1 + 0.60\left(\frac{g_m}{1000}\right)^{1.25}\bar{f}_{l,eff}^{\,0.60}$ $k_{mat} = 1.00$	12.86%	$\bar{f}_{mc} = 1 + 1.10\,\bar{f}_{l,eff}^{\,0.60}$ $k_{mat} = 1.00$	12.73%
Natural Masonry (NM)	22	$\bar{f}_{mc} = 1 + 1.00\left(\frac{g_m}{1000}\right)^{0.15}\bar{f}_{l,eff}^{\,0.40}$ $k_{mat} = 0.40\left(\rho_{mat}\frac{f_{c,mat}}{f_{m0}}\right)^{1.40}$	11.95%	$\bar{f}_{mc} = 1 + 1.05\,\bar{f}_{l,eff}^{\,0.35}$ $k_{mat} = 0.40\left(\rho_{mat}\frac{f_{c,mat}}{f_{m0}}\right)^{1.65}$	11.95%

α_2 and α_3 can be set prudently equal to 1.0, unless experimental results are available to justify different assumptions; α_4 and α_5, instead, are set to 1.81 and 2, respectively.

By following the preliminary outcomes reported in [19], and considering a further increased database, 9 analysis cases were performed to find the strength models fitting the experimental data best. These analysis cases are summarized in Table 1 and differ each other for the number of α_i coefficients made to vary at the same time (1,2,3,4 or 5) while setting the others to constant values as reported in the Table.

Of the 9 cases, 8 are those already considered in [19] (i.e., *Case 1* and from *Case 3* to *Case 9*). Specifically:

- *Case 1* considers the variability in the analyses of all the parameters with the purpose to provide updated values of α_i coefficients in the strength model currently suggested by DT 215 [29];

- *Cases 5* and *6* consider the variability of α_4 and α_5 by setting the remaining parameters to the values calibrated in [33] in the estimate of the compressive strength of masonry columns confined by FRP systems;

- *Cases 3* and *4* derive from *Cases 5* and *6*, respectively, but also consider the variability of α_1;

- *Case 7* considers the variability in α_1 and α_2 by setting α_3, α_4, and α_5 to the values proposed by DT 215 [6] (i.e., $\alpha_3 = 1.00$, $\alpha_4 = 1.81$, and $\alpha_5 = 2.00$);

- *Case 8*, as opposed to *Case 7*, accounts for the variability of α_4 and α_5 by setting α_1, α_2, and α_3 to 0.50, 1.00, and 1.00, respectively, as suggested by DT 215 [6];

- *Case 9* is the only one parameter analysis (α_5) which derives from *Case 5* with the addition of $\alpha_4 = 1.00$.

Finally, *Case 2* is a four-parameter analysis that, by setting $\alpha_3 = 0$, was taken into account in this study with the purpose to compare the calibrated value for α_2 with the value $\alpha_2 = 1.10$ obtained for the case of FRP confinement [33].

In a first step of the proposed study (namely, Step 1), the cases of analysis were applied, one at a time, to three different groups of datasets, i.e.:

- *Group (1)*: all datasets together ($n = 99$), with the aim to find strength models suitable for any masonry type (NM and AM);
- *Group (2)*: datasets related to AM only ($n = 77$);
- *Group (3)*: datasets related to NM only ($n = 22$).

In a second step of the proposed study (namely, Step 2), the same analysis cases were applied, once again, by treating the datasets separately per FRCM system (i.e., B, C, G, PBO and S- FRCM system) but without considering a further distinction between natural and artificial masonry (due to the limitation of available experimental datasets). Objective of this second step of the study is to better examine the strength performance of the confined masonry based on the FRCM type by identifying, for instance, composite systems more effective than others or, even, composites systems for which the same (or similar) strength models can be proposed.

The results of the best-fit analyses are discussed in the following section.

3.1. Step 1: Results of the analyses per masonry type and suitable for any FRCM system

Table 2 provides, for each group of datasets considered in the first step of analyses, the best analytical solutions - labelled *Proposal 1* and *Proposal 2* - obtained from the application of the MAPE minimization technique to the nine examined cases reported in Table 1; the corresponding MAPE values are also provided. *Proposals 1* and *2* account and do not for the contribution of the masonry mass density, respectively.

As noted, in the case of the *Group (1)* (all datasets), *Proposal 1* basically confirms the best-fit model found in [19], with very slight modifications of α_i coefficients. *Proposal 2* provides the coefficient $\alpha_2 = 1.05$ very similar to that found by the authors for the FRP confinement (i.e., 1.05 vs 1.10) [33]; in spite of only a slight strength increase of the MAPE value with respect to *Proposal 1,* the model considers the possibility of neglecting the influence of the inorganic matrix, being $\alpha_5 = 0$. This model is also very similar to *Proposal 2* found for AM, in which $\alpha_2 = 1.10$ and k_{mat} is equal to unit; in particular, *Proposal 2* found for AM is directly comparable to that proposed, for the same masonry type, in the case of FRP confinement [33] with the only exception that the coefficient α_1 is equal to 2/3 (FRCM system, Table 2) against 2/5 (FRP system [33]).

In the case of NM, the found models are a bit more complex, since k_{mat} seems to not assume a constant value and, a straight comparison with the relationships obtained for both the other two groups of datasets and the FRP confined masonry cannot be made. Conversely, based on the obtained MAPE values (basically, the same), the two proposals highlight the possibility of neglecting the contribution of the masonry mass density; indeed, when the contribution of the masonry mass density is considered in the analysis, α_3 is equal to 0.15), thus confirming what already found in the preliminary study [19].

In Fig. 10a, the two proposals suitable for all datasets are plotted together with the experimental $\left(\bar{f}_{mc} - \frac{\bar{f}_{l,eff}}{k_{mat}}\right)$ couples of datasets. In particular, the relationship expressed by *Proposal 1* is plotted for three different g_m values, i.e.: 1500, 1700 and 1900 kg/m^3; similarly, the experimental data related to AM and NM are grouped per range of g_m values.

As shown, most experimental points exhibit $\frac{\bar{f}_{l,eff}}{k_{mat}}$ values lower than 0.4. Also, the distribution of the experimental data differentiated by g_m value does not seem to correctly match with the corresponding relationship plotted by considering a given g_m; in other words, a clear correlation between the compressive strength of the FRCM confined masonry and the masonry mass density cannot be identified based on the available experimental database. As a result, it can be stated that – as a first approximation deriving from the current experimental database - the *Proposal 2* catches the overall phenomenon quite well and, despite the non-negligible scatter of data, represents a suitable and easy to apply model for the FRCM confined masonry.

In Fig. 10b, the theoretical values, $\bar{f}_{mc}^{\,th}$, calculated for the 99

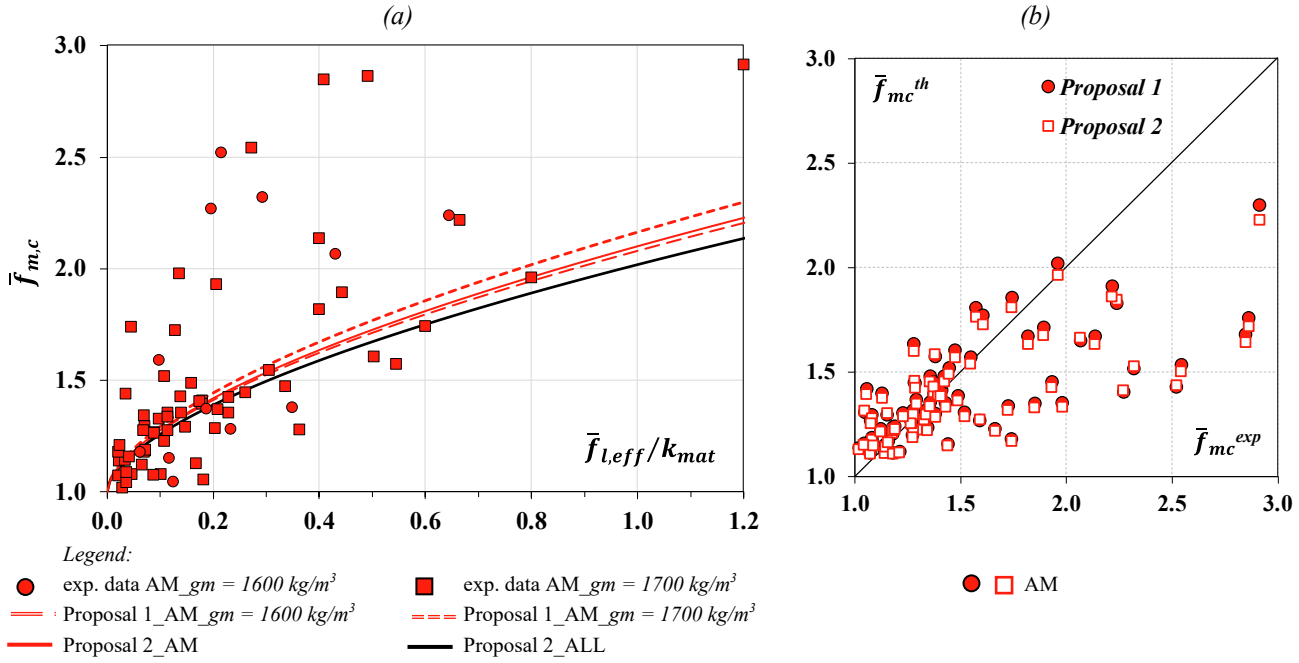

Fig. 11. *Proposal 1* and *2* obtained by considering datasets related to artificial masonry only (a), and comparison between experimental data and predictions (b).

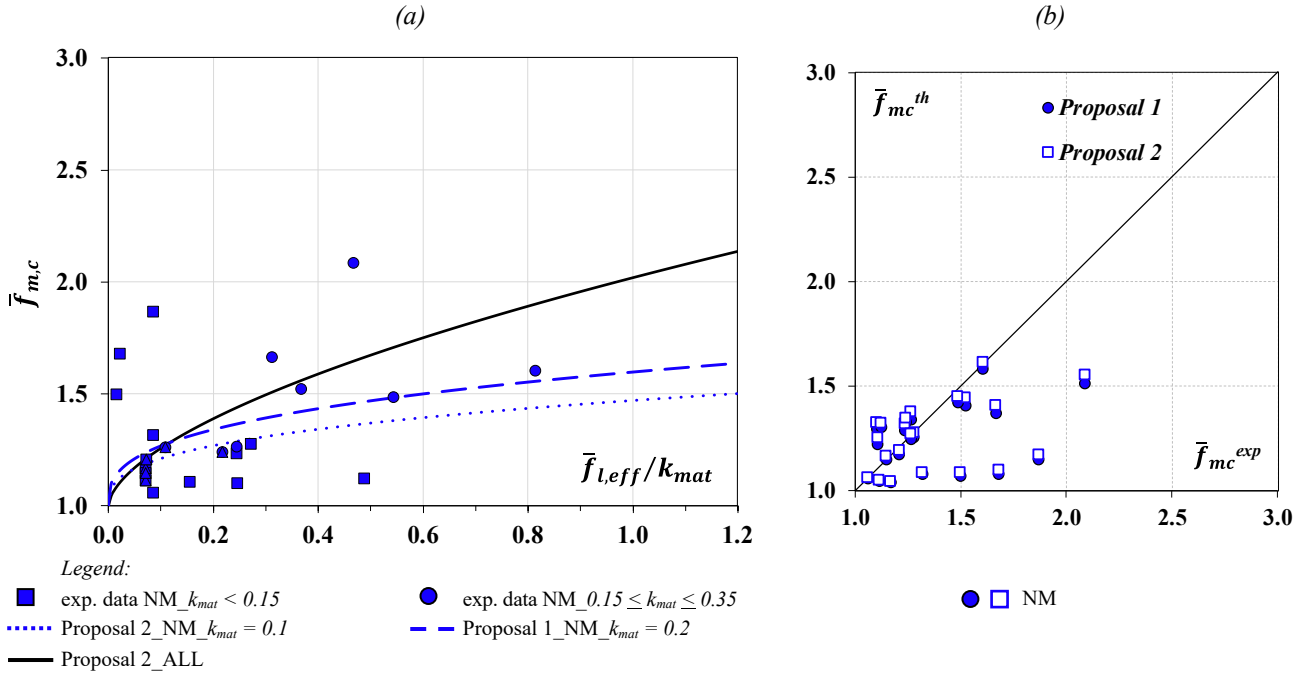

Fig. 12. *Proposal 1* and *2* obtained by considering datasets related to natural masonry only (a), and comparison between experimental data and predictions (b).

datasets according to the two proposals are plotted with respect to the experimental ones, $\bar{f}_{mc}{}^{exp}$. The bisector corresponds to perfect agreement between predictions and tests; therefore, points falling in the lower part of the graph indicate conservative predictions whereas points falling over the line represent unconservative situations. As shown, whatever the proposal, a good number of data are well distributed along the bisector, and another significant set of data is well below the bisector thus indicating conservative predictions; unconservative predictions are also identified but they are in a reduced number and not highly significant in the values.

As a general consideration from Fig. 10 it can be stated that, the high scattering of the experimental results collected in the database is, of course, an issue to the development of more reliable analytical models, and the present proposals are those performing better in terms of error minimization between experiments and predictions. However, it is worth noting that, even though the overall error could be not representative of the possible error on a specific prediction, the choice of preferring to use the MAPE as error minimization technique with respect to counterpart methods assures the development of conservative predictive models, as shown in Fig. 10b.

Fig. 11a,b and 12a,b show plots similar to those of Fig. 10a,b but they focus on Group (2) (AM, $n = 77$) and Group (3) (NM, $n = 22$) of datasets,

Table 3
Strength models per FRCM system.

FRCM system	n	*Proposal 1*		*Proposal 2*	
		Describing Equation	$(E_{rr})_m$	Describing Equation	$(E_{rr})_m$
B-FRCM	13	–	–	$\bar{f}_{mc} = 1 + 1.10\,\bar{f}_{l,eff}^{\,0.40}$ $k_{mat} = 0.55$	11.49%
C-FRCM	25	$\bar{f}_{mc} = 1 + 0.40\left(\frac{g_m}{1000}\right)^{1.90}\bar{f}_{l,eff}^{\,0.70}$ $k_{mat} = 1.00$	9.33%	$\bar{f}_{mc} = 1 + 1.10\,\bar{f}_{l,eff}^{\,0.70}$ $k_{mat} = 0.95$	9.25%
G-FRCM	26	$\bar{f}_{mc} = 1 + 1.65\left(\frac{g_m}{1000}\right)^{1.15}\bar{f}_{l,eff}$ $k_{mat} = 0.90\left(\rho_{mat}\frac{f_{c,mat}}{f_{m0}}\right)^{0.25}$	12.24%	$\bar{f}_{mc} = 1 + 2.35\,\bar{f}_{l,eff}^{\,0.85}$ $k_{mat} = 0.85\left(\rho_{mat}\frac{f_{c,mat}}{f_{m0}}\right)^{0.25}$	12.67%
PBO-FRCM	10	$\bar{f}_{mc} = 1 + 0.55\left(\frac{g_m}{1000}\right)^{3.90}\bar{f}_{l,eff}$ $k_{mat} = 1.00$	10.09%	$\bar{f}_{mc} = 1 + 4.36\,\bar{f}_{l,eff}$ $k_{mat} = 1.00$	10.09%
S-FRCM	25	$\bar{f}_{mc} = 1 + 0.20\left(\frac{g_m}{1000}\right)^{3.90}\bar{f}_{l,eff}^{\,0.80}$ $k_{mat} = 1.00$	8.68%	$\bar{f}_{mc} = 1 + 0.75\,\bar{f}_{l,eff}^{\,0.35}$ $k_{mat} = 0.70$	13.45%

respectively. In particular, in Fig. 11a the experimental $\left(\bar{f}_{mc} - \frac{\bar{f}_{l,eff}}{k_{mat}}\right)$ values, differentiated by g_m, are compared with *Proposal 1* and *Proposal 2* obtained for the case of artificial masonry and, also, with *Proposal 2* suitable for any masonry type. First, the comparison shows the clear similarity among the considered models so that all of them can be suitable proposals for FRCM confined specimens made of artificial masonry. To this purpose, it is worth highlighting that, in the case of AM, *Proposal 1* trivially accounts for the contribution of the masonry mass density since, as mentioned earlier, the value of g_m is almost never indicated in the scientific papers and therefore, for many datasets it has been assumed equal to 1700 kg/m^3; therefore, by roughly replacing this value in *Proposal 1*, the model basically degenerates into *Proposal 2*. For the same reason, the comparison in Fig. 11b shows that, there is no significant difference between *Proposal 1* and *Proposal 2* found for AM, with most points well distributed about the bisector and a good number of them located in the conservative zone.

In Fig. 12a the experimental $\left(\bar{f}_{mc} - \frac{\bar{f}_{l,eff}}{k_{mat}}\right)$ values, differentiated by k_{mat} values, are compared with both *Proposal 2* found for NM and *Proposal 2* suitable for any masonry type. As shown, based on the available experimental database, a clear correlation between k_{mat} and the compressive strength of the FRCM confined masonry cannot be identified; indeed, the distribution of the experimental points does not show a palpable trend with k_{mat}.

Finally, the comparison in Fig. 12b between the accuracy of the predictions obtained by considering both *Proposal 1* and *Proposal 2* found for NM does not show significant differences; therefore, both proposals are suitable and mostly provide conservative predictions.

3.2. Step 2: Results of the analyses per FRCM system

Table 3 provides, for each group of datasets considered in the second step of analyses, the best analytical solutions - labelled *Proposal 1* and *Proposal 2* - obtained from the application of the MAPE minimization technique to the nine examined cases; the corresponding MAPE values are also provided. Again, *Proposals 1* and *2* account and do not for the contribution of the masonry mass density, respectively; indeed, *Proposal 2* does not include the variability of the term $\left(\frac{g_m}{1000}\right)^{\alpha_3}$, since $\alpha_3 = 0$.

For the B-FRCM system, only one model is provided since in the performed analysis, *Proposal 1* degenerates in *Proposal 2*, meaning that the best model in terms of error minimization is always that considering $\alpha_3 = 0$. This is also motivated by the g_m data collection reported in Table A.1 and A.2 where three datasets show values -different from 1700 kg/m^3.

For the PBO-FRCM system, instead, the models fitting the experimental datasets best linearly change with the normalized effective

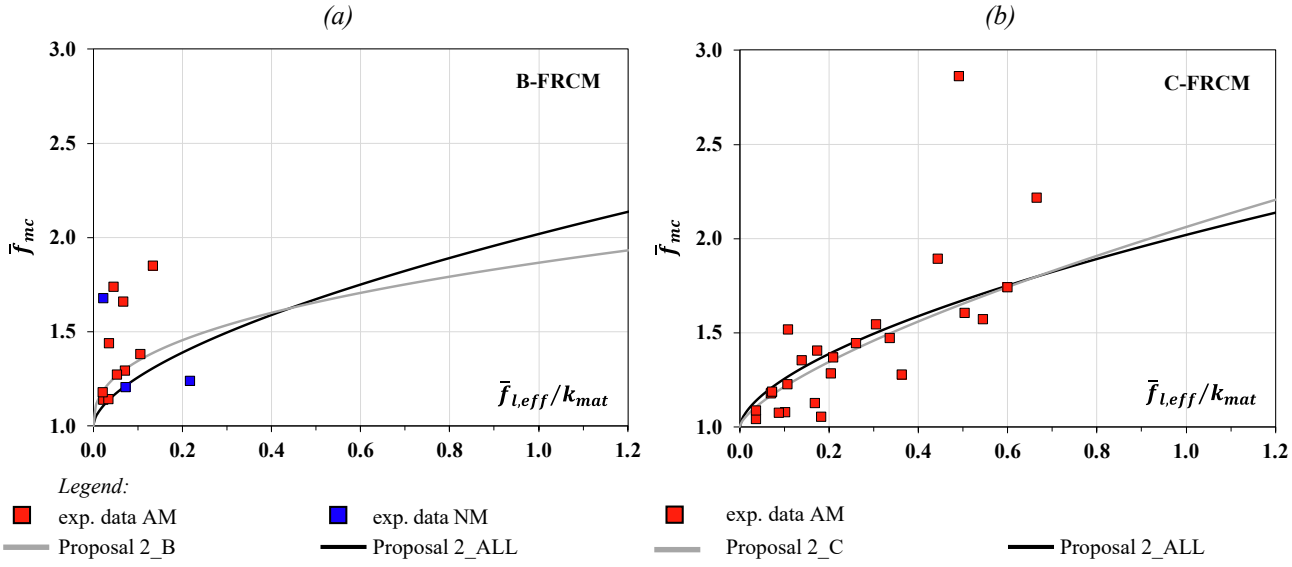

Fig. 13. *Proposal 1* and *2*: B-FRCM system (a), and C-FRCM system.

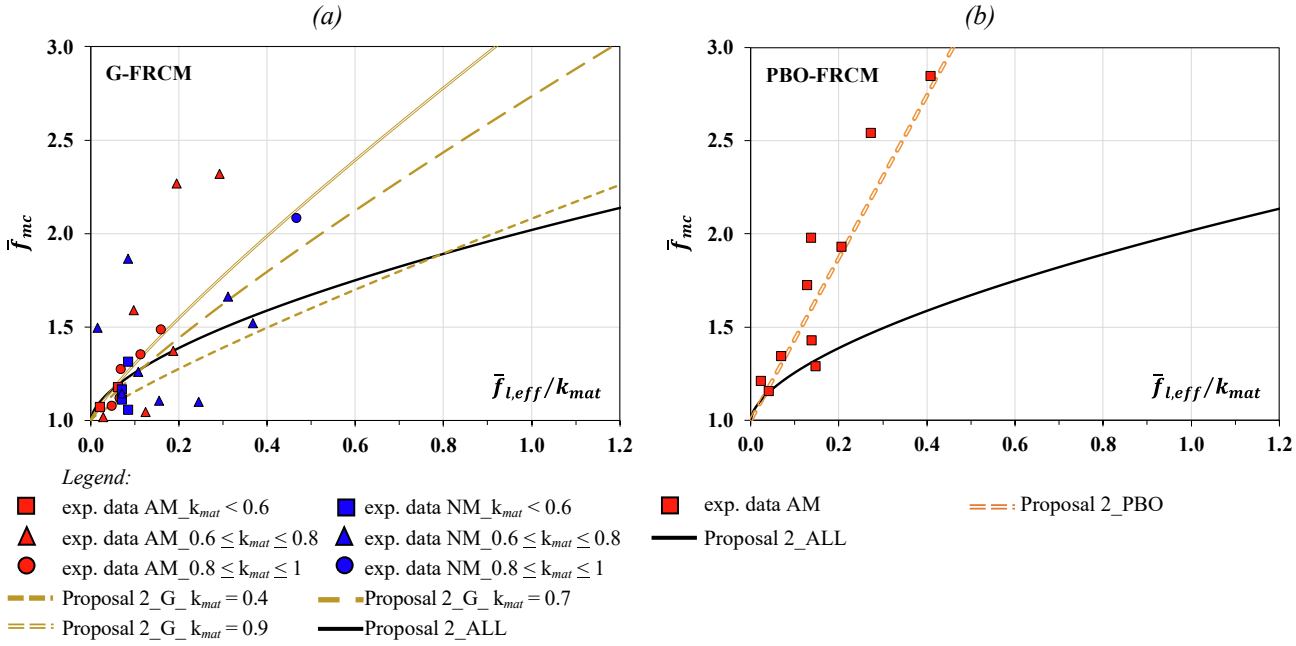

Fig. 14. *Proposal 1* and *2*: G-FRCM system (a), and PBO-FRCM system.

confining pressure being $\alpha_1 = 1$ (see Eq. (3)).

Except for the G-FRCM system, all the models neglect the dependence of k_{mat} on the masonry compressive strength, since the performed analyses always yielded $\alpha_5 = 0$. This means that, based on Eq. (5), these models are not affected by the change of the values assumed by the parameters ρ_{mat} and $\frac{f_{mat,c}}{f_m}$ from which k_{mat} depends on. This result may seem to be in conflict with what it is known in the literature, since it has been frequently experienced that the early or delayed cracking of the inorganic matrix has an influence on the overall behaviour of the FRCM confined masonry under compression [32,42]. To this purpose, the authors are firmly aware that the matrix properties is an important parameter in the FRCM systems; however, at the same time, establishing the criteria through which it is possible to predict the structural performance of the confined member based on the available data is very hard and, maybe, the parameter k_{mat} is not the most suitable means.

Indeed, the analysis of the influence of the mortar shall always be coupled with other parameters, such as the geometry of the mesh (with more or less dense fibers) and the compressive strength of the masonry. However, given the heterogeneity of data currently available in the database, the effective influence of the mortar seems to be not visible in the proposed models which purpose is to simulate, on average, the strength performance of confined members.

Fig. 13a and 13b show the comparison between the experimental $\left(\bar{f}_{mc} - \frac{\bar{f}_{l,eff}}{k_{mat}}\right)$ values and the *Proposal 2* specifically derived for the case of B- and C- FRCM systems, respectively; for a better comparison, *Proposal 2* suitable for any FRCM system is also plotted in both figures.

Mainly for the C-FRCM system (Fig. 13b), there is no significant difference between the companion models - namely *Proposal 2_C (or B)* and *Proposal 2_ALL* – so that the general model suitable for any fiber type can be successfully applied for these two systems. Also, in the case of the C-FRCM system, all datasets include confined specimens made of AM for which $g_m = 1700$ kg/m^3 is always applicable. As a result, *Proposal 1* in Table 3 trivially degenerates into *Proposal 2* and, therefore, it is not plotted in Fig. 13b.

Fig. 14a and 14b show the comparison between the experimental $\left(\bar{f}_{mc} - \frac{\bar{f}_{l,eff}}{k_{mat}}\right)$ values and the *Proposal 2* specifically derived for G- and PBO- FRCM systems, respectively; for a better comparison, *Proposal 2* suitable for any FRCM system is also plotted in both figures.

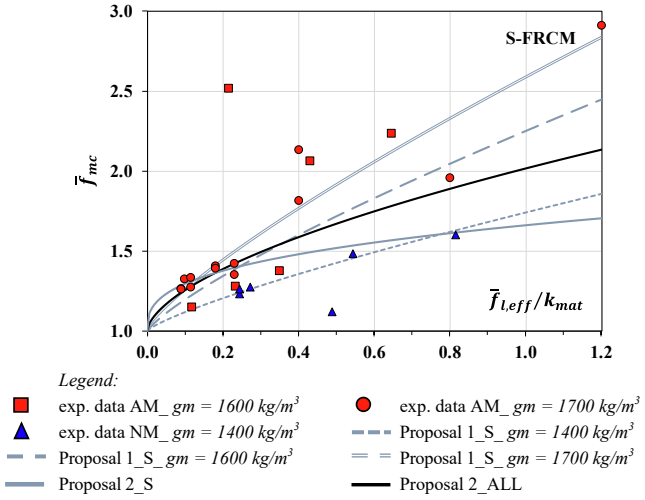

Fig. 15. *Proposal 1* and *2*: S-FRCM system.

For the G-FRCM system (Fig. 14a), *Proposal 2* has been plotted by considering three different values of k_{mat} (i.e., 0.4, 0.7 and 0.9) which were chosen based on the variability of such parameter within proper k_{mat} ranges identified among the experimental datasets. Also in this case, a clear correlation between k_{mat} and $\bar{f}_{mc}$ is not strictly identified; the distribution of experimental datasets per k_{mat} about the plotted relationships seems rather random.

By focusing on the PBO-FRCM system (Fig. 14b), it is noted a significant difference between the companion models - namely *Proposal 2_PBO* and *Proposal 2_ALL* – so that the general model found for any fiber type does not seem to be successfully applicable to this system, mainly under $\frac{\bar{f}_{l,eff}}{k_{mat}}$ values higher than 0.2. Even though the available datasets for the PBO-FRCM system are only 10 and, therefore, the obtained result needs a deeper investigation in future, the plot highlights a better performance of this system with respect to the others and a clear correlation of the normalized compressive strength with $\bar{f}_{l,eff}$. The motivation is not

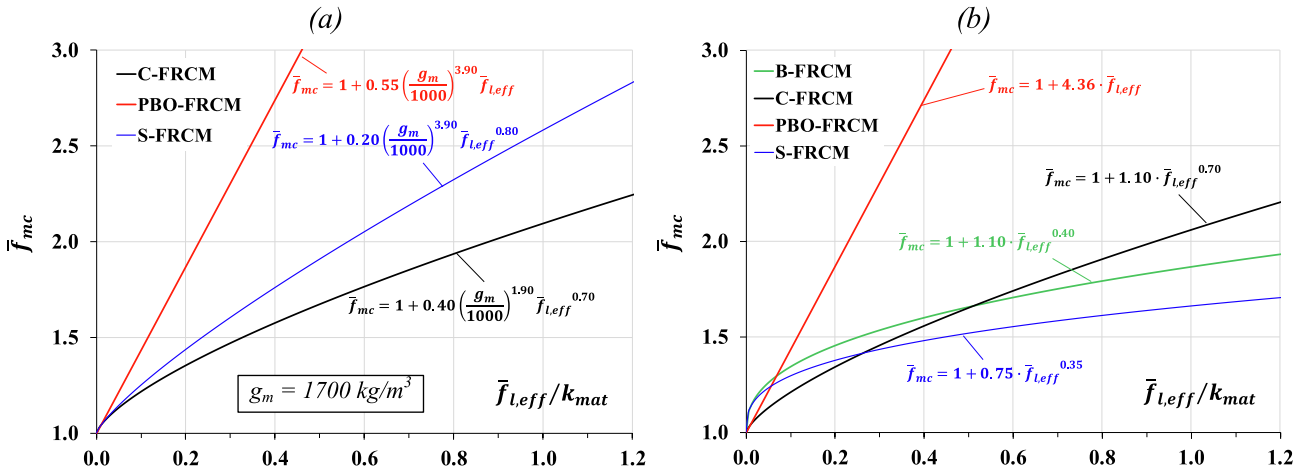

Fig. 16. Comparison among the FRCM systems in terms of *Proposal 1* (a) and *Proposal 2* (b).

evident but, looking at the database in Table A.1, it may seem that the values of the mechanical and geometrical parameters characterizing the considered datasets are less scattered. Furthermore, like the C-FRCM system, all the collected datasets include confined specimens made of AM for which $g_m = 1700$ kg/m^3 is always applicable. As a result, *Proposal 1* in Table 3 trivially degenerates into *Proposal 2* and, therefore, it is not plotted in Fig. 14b.

Fig. 15 shows the comparison between the experimental $\left(\bar{f}_{mc} - \frac{\bar{f}_{l,eff}}{k_{mat}}\right)$ values and both *Proposal 1* and *Proposal 2* specifically derived for the S-FRCM system; furthermore, for a better comparison, *Proposal 2* suitable for any FRCM system is reported. *Proposal 1* has been plotted by considering three different values of g_m (i.e., 1400, 1600 and 1700 kg/m^3) corresponding to the values identified among the 25 collected datasets.

With respect to the other FRCM systems, a clearer correlation between the g_m values characterizing the experimental datasets and *Proposal 1* is identified, with data related to NM well distributed about the relationship plotted by considering $g_m = 1400$ kg/m^3. Also in this case, most experimental points are concentrated towards $\frac{\bar{f}_{l,eff}}{k_{mat}}$ values lower than 0.4 where both *Proposal 2_S* and *Proposal 2_ALL* provide accurate predictions.

Finally, in Fig. 16a and 16b the models found for the considered FRCM systems are compared. In particular, the comparison in Fig. 16a is related to the models "*Proposal 1*" i.e., to those accounting for the contribution of the masonry mass density g_m ($g_m = 1700$ kg/m^3 has been assumed in the figure), while the plot in Fig. 16b refers to the more simplified models "*Proposal 2*". In both figures, the models obtained for the G-FRCM systems are not plotted because they also account for the variability of the parameter k_{mat}.

From the figures it is observed that, concerning *Proposal 1*, the models found for the various FRCM systems differ from each other; for a given $\frac{\bar{f}_{l,eff}}{k_{mat}}$ ratio, the best performance is provided by the linear relationship found for the PBO-FRCM system. Concerning *Proposal 2*, the PBO model provides, again, the best performance, while the relationships obtained for the other systems are more similar to each other; in particular, a unique relationship may be suggested for the B- and S-FRCM systems.

4. Comparison with design guidelines

The accuracy of the proposed models in Table 2 and Table 3 was compared with the suitability of the analytical formulas suggested by the mentioned guidelines CNR-DT 215 [29] and ACI 549.6R [30]. In particular, the latter guide is the result of the work carried out by ACI 549-L Committee and the RILEM Committee TC 250-CSM, in which design indications are provided according to both American (ACI) and European approaches (RILEM); consequently, two different formulations are given in the guide, provided in Table 4 together with the model by CNR-DT 215 [29] which is reported again for a better understanding.

As shown, the model following the "ACI approach", labelled here ACI 549.6R_1, is very similar to the formulation suitable for FRP applications [58]; the model following the "European approach", labelled here ACI 549.6R_2, has a structure more similar to that adopted by CNR-DT 215 [29], since it considers the contribution of the inorganic matrix even though it neglects the influence of the masonry mass density.

The bar charts in Fig. 17a,b,c show the model errors in terms of MAPE values calculated by applying the mentioned formulations to either the 99 datasets together (Fig. 17a) or treating artificial (Fig. 17b) and natural masonry (Fig. 17c) separately. In particular, in Fig. 17b the model errors were calculated by considering both the proposals specifically found for AM (namely, Proposal 1_AM and Proposal 2_AM) and the general ones found for all datasets (namely, Proposal 1_ALL and Proposal 2_ALL). A similar comparison is provided in Fig. 17c where the proposals specifically found for NM are labelled Proposal 1_NM and Proposal 2_NM.

It is worth highlighting that the code formulations were applied to the considered datasets without introducing both the safety factors to use for design purposes and the limitations for the ultimate tensile failure of the fiber mesh $\varepsilon_{f,u}$.

From the plots it is noted that new proposals provide the best predictions, followed by the models suggested by CNR-DT 215 [29] and by the model ACI 549.6R_1 [30]; the less accurate estimates are provided by the formulation labelled ACI 549.6R_2 [30], with errors up to 81% in the case of NM; however, it is common to all the guidelines' formulas that the less accurate predictions are obtained in the case of NM, probably due to the lack of experimental data available at the time of their validation which, instead, will have been mostly based on AM. Finally, the comparisons in Fig. 17 allow for validating the accuracy of the general models proposed for any type of masonry (Proposal 1_ALL and Proposal 2_ALL) since, based on the model errors, they can be successfully applied for the case of natural and artificial masonry.

Bar charts like those in Fig. 17 are shown in Fig. 18 where the MAPE values were calculated by separating the datasets per FRCM system. Again, for each group of datasets, the accuracy of both guidelines' formulas and proposed models - the latter developed with reference to all datasets and to those of the given FRCM system – is examined.

Overall, the model by CNR-DT 215 [29] provides rather good estimates whatever the FRCM system, with the most accurate predictions in the case of glass (MAPE error = 18%, Fig. 18c) and PBO (MAPE error = 17.5, Fig. 18d) fibers. Conversely, the model ACI 549.6R_1 [30] provides

Table 4
Summary of the strength models available in the literature or in international guidelines*.

Guidelines	*Normalized effective confining pressure,* $\bar{f}_{l,eff} = \frac{f_{l,eff}}{f_m}$	*MODEL,* $\bar{f}_{mc} = \frac{f_{mc}}{f_m}$
ACI 549.6R [30] *"ACI approach"*	$\bar{f}_{l,eff} = k_H\, k_V\, \frac{f_l}{f_m} = k_H\, k_V\, \frac{\frac{1}{2} \bullet \rho_f \bullet E_f \bullet \varepsilon_{f,u}}{f_m} k_H =$ $\begin{cases} 1 \,(circular sections) \\ \left(\frac{B}{H}\right)^2 \left[1 - \frac{\left[\left(\frac{B}{H}\right)(H-2r_c)^2 + \left(\frac{H}{B}\right)(B-2r_c)^2\right]}{3 \bullet (B \bullet H)}\right] (rectangular sections) \end{cases}$ $k_V = \begin{cases} 1 \quad (\text{continuous wrapping}) \\ \left(1 - \frac{p_f'}{2 \cdot D}\right)^2 \\ 1 - \frac{p_f'}{2 \cdot \min(B,H)} \end{cases} (\text{discontinuous wrapping}) \begin{cases} (\text{circular sections}) \\ (\text{rectangular section}) \end{cases}$ $\rho_f = \begin{cases} 4\frac{t_f}{D} (circular sections) \\ 4\frac{t_f}{\sqrt{B^2+H^2}} (rectangular sections) \end{cases}$ B = *short side dimension of the rectangular cross-section* H = *long side dimension of the rectangular cross-section*	$\bar{f}_{mc} = 1 + 3.30\, \bar{f}_{l,eff}$
ACI 549.6R [29] *"European approach"*	$\bar{f}_{l,eff} = k_H\, k_V\, \frac{f_l}{f_m} = k_H\, k_V\, \frac{\frac{1}{2} \bullet \rho_f \bullet E_f \bullet \varepsilon_{f,u}}{f_m} k_H =$ $\begin{cases} 1 \,(circular sections) \\ \left(\frac{B}{H}\right)^2 \left[1 - \frac{\left[\left(\frac{B}{H}\right)(H-2r_c)^2 + \left(\frac{H}{B}\right)(B-2r_c)^2\right]}{3 \bullet (B \bullet H)}\right] (rectangular sections) \end{cases}$ $k_V = \begin{cases} 1 \quad (\text{continuous wrapping}) \\ \left(1 - \frac{p_f'}{2 \cdot D}\right)^2 \\ 1 - \frac{p_f'}{2 \cdot \min(B,H)} \end{cases} (\text{discontinuous wrapping}) \begin{cases} (\text{circular sections}) \\ (\text{rectangular section}) \end{cases}$ $\rho_f = \begin{cases} 4\frac{t_f}{D} (circular sections) \\ 4\frac{t_f}{\sqrt{B^2+H^2}} (rectangular sections) \end{cases}$ B = *short side dimension of the rectangular cross-section* H = *long side dimension of the rectangular cross-section*	$\bar{f}_{mc} = 1 + k\, \bar{f}_{l,eff}^{0.50} k = 6\rho_{mat} \frac{f_{mat,c}}{f_m} \rho_{mat} =$ $\begin{cases} \frac{4 \bullet t_{mat}}{D} (circular sections) \\ \frac{4 \bullet t_{mat}}{\sqrt{B^2+H^2}} (rectangular sections) \end{cases}$
CNR-DT 215 [29]	$\bar{f}_{l,eff} = k_H\, k_V\, \frac{f_l}{f_m} = k_H\, k_V\, \frac{\frac{1}{2} \bullet \rho_f \bullet E_f \bullet k_{mat} \bullet \varepsilon_{f,u}}{f_m} k_H =$ $\begin{cases} 1 \,(circular sections) \\ 1 - \frac{\left[(H-2r_c)^2 + (B-2r_c)^2\right]}{3 \bullet (B \bullet H)} (rectangular sections) \end{cases}$ $k_V = \begin{cases} 1 \quad (\text{continuous wrapping}) \\ \left(1 - \frac{p_f'}{2 \cdot D}\right)^2 \\ 1 - \frac{p_f'}{2 \cdot \min(B,H)} \end{cases} (\text{discontinuous wrapping}) \begin{cases} (\text{circular sections}) \\ (\text{rectangular section}) \end{cases}$ $\rho_f = \begin{cases} 4\frac{t_f}{D} (circular sections) \\ 4\frac{t_f}{\sqrt{B^2+H^2}} (rectangular sections) \end{cases}$	$\bar{f}_{mc} = 1 + \left(\frac{g_m}{1000}\right) \bar{f}_{l,eff}^{0.50} k_{mat} = 1.81 \left(\rho_{mat} \frac{f_{mat,c}}{f_m}\right)^2 \leq$ $1\rho_{mat} = \begin{cases} \frac{4 \bullet t_{mat}}{D} (circular sections) \\ \frac{4 \bullet t_{mat}}{\sqrt{B^2+H^2}} (rectangular sections) \end{cases}$

* See the section "Nomenclature" for the meaning of symbols.

good estimates in the case of basalt (MAPE error = 16.6%, Fig. 18a), glass (MAPE error = 16.8%, Fig. 18c) and PBO (MAPE error = 15.3%, Fig. 18d) fibers and less reliable predictions for carbon (MAPE error = 26.7%, Fig. 18b) and steel fibers (MAPE error = 39.2%, Fig. 18e).

The alternative model ACI 549.6R_2 [30], instead, seems to provide the less accurate estimates, particularly for the case of C- (MAPE error = 93.2%, Fig. 18b) and G-FRCM system (MAPE error = 65.8%, Fig. 18c) while errors lower than 30% were found only in the case of basalt fibers

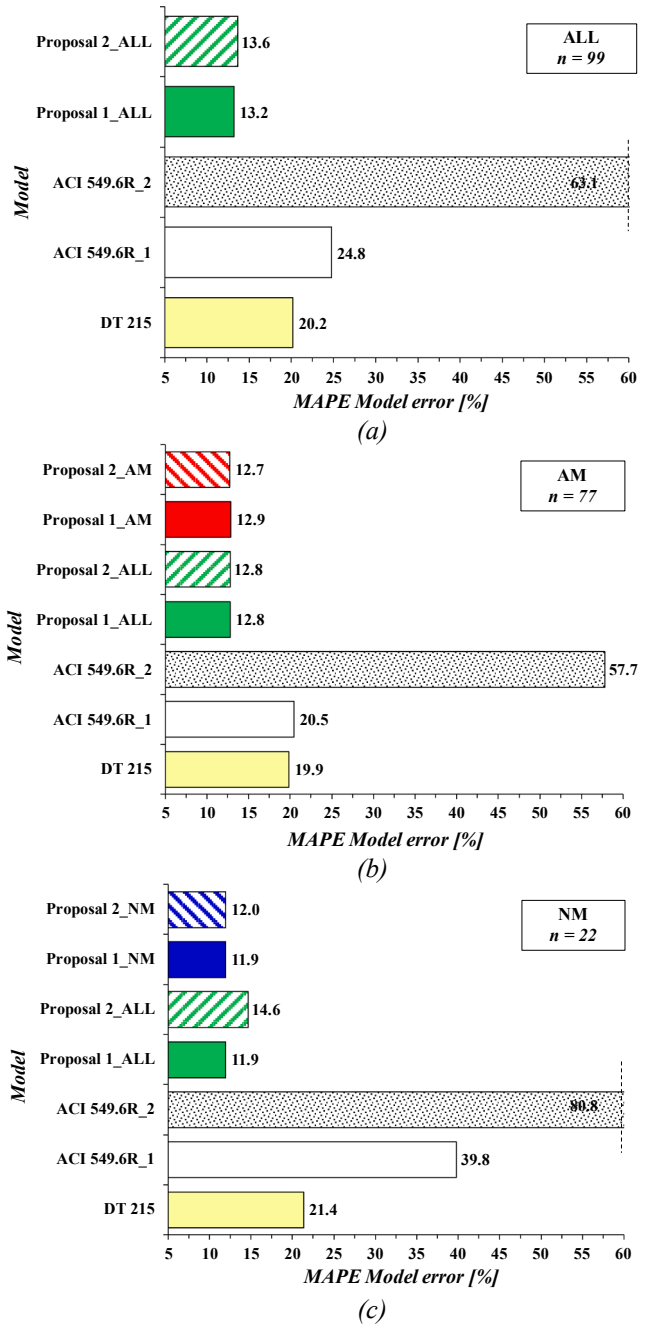

Fig. 17. Accuracy of strength models: a) all datasets; b) datasets related to AM; c) datasets related to NM.

(MAPE error = 28.7%, Fig. 18a). Even though the overall less accuracy of this model needs more investigation in future, a reason could rely on the estimate of the k parameter ($=6\rho_{mat}\frac{f_{mat,c}}{f_m}$) which directly multiplies the normalized effective confinement. According to the authors, k should be limited to a maximum value to be properly identified. Indeed, for significantly high values assumed by ρ_{mat} or, especially, by $\frac{f_{mat,c}}{f_m}$ or by their product, the k value might significantly affect the prediction of the normalized compressive strength which can reach so high values to be unrealistic. Conversely, concerning the good accuracy of the model by CNR-DT 215 [29], it can be observed that, the parameter k_{mat} has the same structure of the parameter k in the formulation by ACI 549.6R_2 [30] but its influence is limited to 1 (i.e., $k_{mat} \leq 1$, see Eq. (1) or Table 4). The meaning of k_{mat}, indeed, should be to reduce the efficiency of the confining jacket in cases of non-optimal geometric and mechanical conditions related to the inorganic matrix; this is the reason for which k_{mat} is directly reported in the analytical expression of the lateral confining pressure (see Eq. (4) or Table 4).

As expected, the models specifically found for each FRCM system provide the best estimates; however, the general formulations suitable for any fiber type (Proposal 1_ALL and Proposal 2_ALL) also yield good predictions, and only in the case of the G- and PBO- FRCM systems the MAPE errors approach 20%.

5. Conclusions

In this paper, research advances performed by the authors on the compressive strength of masonry columns confined with FRCM composites have been presented. The performed analytical study was based on a wide experimental database compiled from the literature and including the results of 261 compression tests on masonry members confined by FRCM, most of which with square or rectangular cross-section and only 28 with circular cross-section.

A reduced number of members was made of natural blocks (tuff units or limestone) while the majority of them was manufactured by properly assembling clay bricks.

The collected database was a valuable tool to provide an overview about the scatter of values assumed by some key geometric and mechanical parameters investigated in the experimental studies and useful for the subsequent development of strength models. The analysis has shown that, regardless of the masonry mass density g_m, the values of such parameters are quite scattered by varying the FRCM confinement system and, thus, examining the influence of these parameters on the compression strength is a challenging task. Concerning the parameter g_m, instead, an in-depth study on its effect on the compressive strength f_{mc} was not possible on the basis of the available data; indeed, the values of the masonry mass density investigated in the experimental studies were often not indicated in the scientific papers, mainly in the case of clay brick masonry specimens which represent the majority of collected members.

Several analysis cases were taken into account in order to find sound formulas to estimate the compressive strength of the FRCM confined masonry. The relationships were found by best-fitting the experimental test results which were preventively organized in homogeneous datasets.

The first step of the analytical study focused on the development of strength models both suitable for any masonry type (natural and artificial) and specifically applicable to artificial masonry (AM) only or natural masonry (NM) only. From those analyses, the following main conclusions were drawn:

- overall, the compressive strength of the FRCM confined masonry, whatever the masonry type, can be predicted by an easy – to – apply relationship which does not account for the contribution of both masonry density and inorganic matrix's properties; the structure of this formula is very similar to that found by the authors in a previous study on the FRP confinement of masonry and, also, to the relationships specifically derived by considering only datasets related to AM.

- a better investigation is needed in future studies for the case of NM, for which the datasets available so far are very few and the obtained results require a more in-depth analysis.

The second step of the analytical study focused on the development of strength models better suitable for the specific fiber type investigated in the FRCM system (basalt - B, carbon - C, glass - G, PBO and steel - S), but without considering a further distinction between natural and artificial masonry. From those analyses, it has been found that a unique relationship may be suggested for the B- and S- FRCM systems, while the strength model found for the PBO-FRCM system seems to provide the best performance.

The last step of the study focused on comparing the accuracy of the models predictions with the analytical estimates obtained by using the

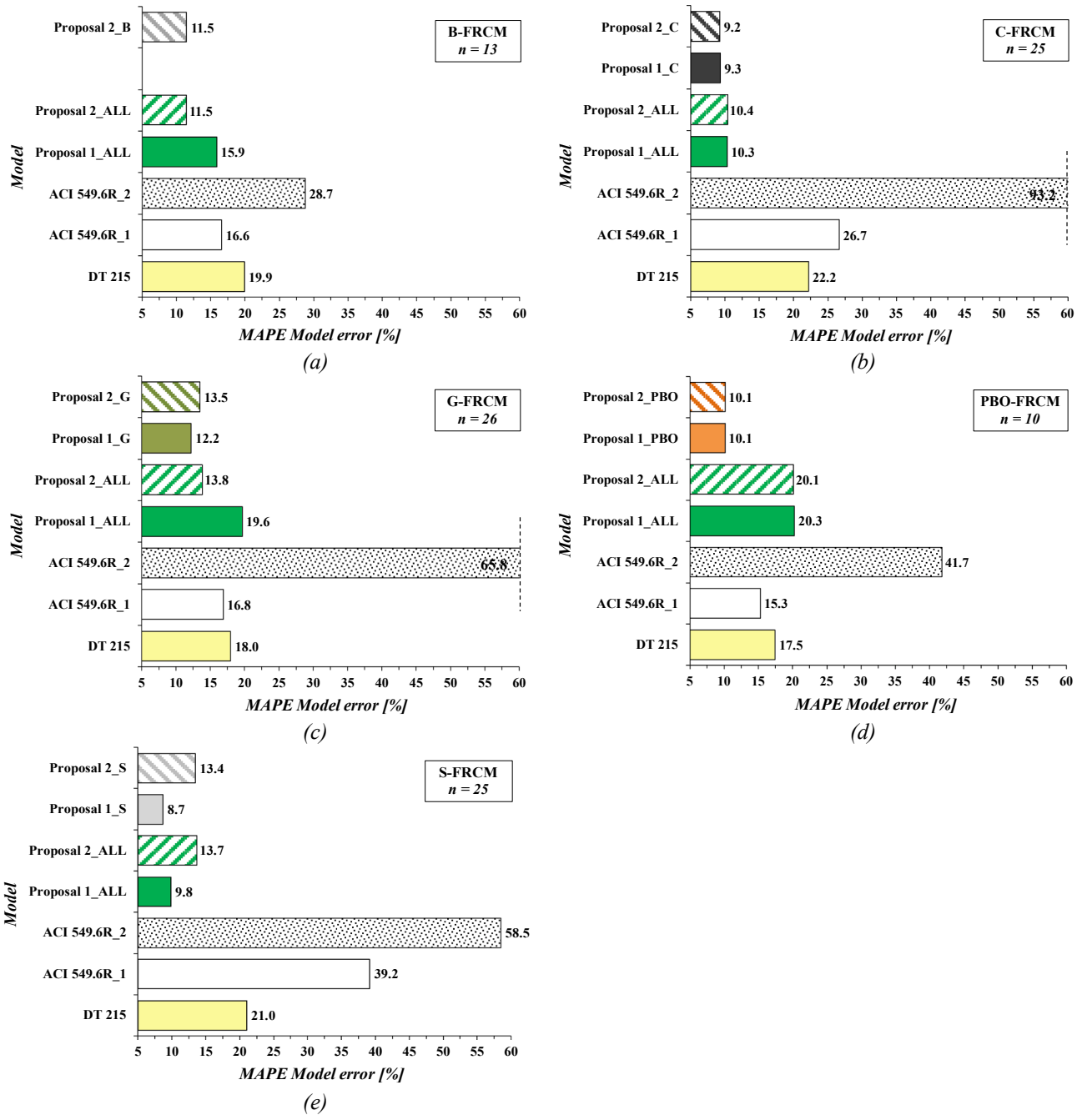

Fig. 18. Accuracy of strength models: a) B-FRCM; b) C-FRCM; c) G-FRCM; d) PBO-FRCM; e) S-FRCM.

formulations suggested by the Italian guidelines CNR-DT 215/2018 and by the American guide ACI 549.6R/2020 (this guide provides two alternative relationships). The following observations were made:

- the new proposals provide the best predictions (model errors in the range 12–14%), followed by the models suggested by CNR-DT 215 (model errors about 20–21%) and by the model ACI 549.6R which neglects the inorganic matrix's properties (model errors in the range 20–40%); the less accurate estimates are provided by the alternative formulation provided ACI 549.6R which accounts for the inorganic matrix's properties, with errors up to 81% in the case of NM; however, it is common to all the guidelines' formulas that the less accurate predictions are obtained in the case of NM, probably due to the lack of experimental data available at the time of their validation which, instead, will have been mostly based on AM.

- as expected, the models specifically found for each FRCM system provide the best estimates; however, the general formulations suitable for any fiber type also yield good predictions, and only in the case of the G- and PBO- FRCM systems the MAPE errors approach 20%.

- overall, the model by CNR-DT 215 provides rather good estimates whatever the FRCM system, with the most accurate predictions in the case of G and PBO fibers (model errors about 17–18%).

- in the case of basalt, glass and PBO fibers, good predictions are also provided by the model ACI 549.6R which neglects the inorganic matrix's properties (model errors about 15–17%).

In continuity to the study presented here, it is worth mentioning that the development of analytical formulas for the prediction of the ultimate strain is ongoing by the authors. Then, a comparison in terms of reliability with the few formulas published in the literature or reported in international guidelines will be performed. To this purpose, it is highlighted that Guidelines CNR-DT 215 do not currently provide indications

about the estimate of the ultimate strain of the FRCM confined masonry, and the study under preparation may represent a first attempt to provide a contribution to the mentioned document. In carrying out the work, the possibility of applying machine learning regression to fit the experimental test data will be also examined.

CRediT authorship contribution statement

Annalisa Napoli: Conceptualization, Data curation, Formal analysis, Investigation, Methodology, Validation, Visualization, Writing – original draft. **Roberto Realfonzo:** Funding acquisition, Supervision, Visualization, Writing – review & editing.

Declaration of Competing Interest

The authors declare that they have no known competing financial interests or personal relationships that could have appeared to influence the work reported in this paper.

Data availability

Data will be made available on request.

Acknowledgements

The financial support by ReLUIS (Network of the Italian University Laboratories for Seismic Engineering - Italian Department of Civil Protection) is gratefully acknowledged (Executive Project 2022-24 - WP14).

Appendix A:. Description of the database and details

The main details of 116 datasets collected from the literature are provided in Table A.1 and Table A.2 for the case of prismatic and cylindrical specimens, respectively. Each dataset has been identified by following the "Design by testing" approach recommended by the Annex D of Eurocode 0 [54]. In particular, it is representative of a group of N experimental tests performed by same researchers and characterized by uniformity in terms of:

a) material and masonry arrangement (*type*, g_m and *scheme*),
b) specimen size (B, H, L and r_c for square/rectangular columns; D and L for circular columns),
c) geometry, typology of FRCM system and confinement layout (γ_f, $t_{f,j}$, n_f, L_b, k_V and k_H),
d) mechanical properties of the fiber mesh ($f_{f,u}$, E_f and $\varepsilon_{f,u}$),
e) thickness (t_{mat}) and mechanical properties of the inorganic matrix employed in the FRCM system ($f_{mat,c}$, $f_{mat,b}$ and E_{mat});
f) compressive strength of the unconfined masonry (f_m);

The experimental result attributed to each dataset, provided in Table A.1 and A.2 in terms of compressive strength of the FRCM confined masonry f_{mc}, normalized with respect to f_m (i.e.,$\frac{f_{mc}}{f_m}$), represents the average value calculated from the collected N tests; for more details, reference to [19] can be made.

In detail, for each dataset the following information is reported in Table A.1 and Table A.2:

a) the reference to the manuscript ("*source*") from which the experimental data were obtained;
b) the nature of masonry (*type*), its mass density (g_m), the compressive strength of the unconfined masonry (f_m), and the arrangement of the masonry units in both plan and elevation (*scheme*) of the member. The latter information is applicable to prismatic specimens only and can be found in [19]; in particular, five layouts were identified based on the number of bricks and mortar joints employed in the cross-section, and none of those schemes indicate hollow sections. It is noted that when the mass density has not been found in the literature papers, a typical average value of g_m for that type of masonry has been assumed and indicated in the tables (in such cases the g_m values are reported in italics);
c) the label of each single dataset, *"ID"*;
d) the number "*N*" of tests grouped under the same dataset;
e) the geometry of each specimen (B, H and r_c are, respectively, the width, the depth and the corner radius of the rectangular cross-section; D is the diameter of the circular cross-section; L is the height of the column);
f) the mechanical and geometric properties of the inorganic matrices (E_{mat}, $f_{mat,c}$, $f_{mat,b}$) are, respectively, the elastic modulus in compression, the compressive strength and the bending strength of the matrix, while t_{mat} is the overall thickness of the FRCM jacket;
g) the type *(BD = bidirectional; UD = unidirectional)* and the properties of the fabric meshes (γ_f, $f_{f,u}$, E_f, $\varepsilon_{f,u}$, and $t_{f,j}$) are, respectively, the density, the tensile strength, the elastic modulus and the ultimate strain of the dry strengthening sheet, and the equivalent thickness of the single layer);
h) the number (n_f) and the overlapping length (L_b) of the FRCM layers;
i) the coefficients of horizontal and vertical confinement efficiency (k_H and k_V, respectively), the former calculated according to the guidelines DT 215 [29] and the latter estimated as suggested by DT 200 R1 [55];
j) the strain efficiency factor (k_ε) of the FRCM system attributed to the dataset, information available only for a few datasets performed on FRCM confined specimens with circular cross-section. It is defined as the ratio between the ultimate hoop strain experimentally measured in the FRCM jacket ($\varepsilon_{j,u}$) – obtained by averaging the values available from each test included in the dataset – and the ultimate strain found from fiber coupon tensile tests ($\varepsilon_{f,u}$);
k) the main experimental test result in terms of $\frac{f_{mc}}{f_m}$ and the dominant failure mode exhibited by test specimens (*FM*), i.e.: jacket failure (JF), debonding of the reinforcement at the overlap region (DB) and fiber–matrix slippage (S).

For each of the five investigated FRCM confining systems, the bar charts in Fig. A.1 display the distribution of the values available for some main parameters (1 geometrical and 2 mechanical) of the tests included in the 99 datasets. Particularly, each plot shows the number of datasets in function of the range of values assumed by the following parameters:

Table A1
Experimental database organized per datasets: FRCM confined specimens with square and rectangular cross-section (108 datasets).

Source	Masonry			Specimens						Strengthening												Results	
										Matrix's properties				Fabric mesh's properties						Jacket					
	Type	g_m	*Scheme* [12]	*Dataset ID*	*N*	*B*	*H*	*L*	r_c	f_m	$f_{mat,c}$	$f_{mat,b}$	E_{mat}	t_{mat}	*type*	γ_f	$f_{f,u}$	E_f	$\varepsilon_{f,u}$	$t_{f,j}$	n_f	L_b	k_V	k_H	f_{mc}/f_m	FM
		[kg/m^3]			[-]	[mm]	[mm]	[mm]	[mm]	[MPa]	[MPa]	[MPa]	[GPa]	[mm]	[-]	[g/m^2]	[MPa]	[GPa]	[%]	[mm]	[-]	[mm]	[-]	[-]	[-]	
B-FRCM systems																									
[35]	CB	*1700*	1a	M1_BF_1,2	2	230	230	960	20	4.68	0.55	0.44	-	10	BD	250	1542	89.00	1.80	0.039	1	460	1.00	0.55	1.74	JF
				M3_BF_1,2	2					9.42	4.54	3.13	-	10							1	460	1.00	0.55	1.14	JF
[36]	CB	*1700*	4	S-2B-L (1), (2)	2	360	360	900	12	1.61	0.87	-	-	18	BD	170	-	370.00	1.62	0.046	2	360	1.00	0.42	1.10	JF
				S-2B-F (1), (2)	2						9.83	-	-	18							2	360	1.00	0.42	1.04	JF
			5	R-2B-L (1), (2)	2	630	360	900	12	1.45	0.87	-	-	18							2	360	1.00	0.42	0.99	JF
				R-2B-F (1), (2)	2						9.83	-	-	18							2	360	1.00	0.29	1.00	JF
[37]	LS	1600	3	S_Bgrid	1	400	400	2100	20	4.78	13.61	15.54	-	15	BD	250	1602	89.00	1.80	0.039	1	100	1.00	0.46	1.68	DB
[38]	CB	*1700*	1a	C-B-R-1, 2, …5	5	250	250	770	20	4.87	15.00	-	-	10	BD	200	1700	70.00	2.43	0.032	1	100	1.00	0.53	1.14	JF
				C-B-S-1, 2, …5	5	250	250	770	0												1	100	1.00	0.33	1.18	JF
[39]	CB	*1700*	1a	C-B-1	1	250	250	770	20	5.35	12.85	2.65	-	6	BD	-	930	70.30	1.40	0.064	1	-	1.00	0.53	1.44	DB-JF
				C-B-2	1									9							2	-	1.00	0.53	1.29	DB-JF
[40]	CB	*1700*	1a	A_B3	1	215	215	670	20	9.97	37.80	9.30	-	20*	BD	220	-	89.00	-	0.037	3	195	1.00	0.56	1.15	JF
				A_B5	1									30*							5	195	1.00	0.56	1.31	JF
				A_B7	1									40*							7	195	1.00	0.56	1.44	JF
			1c	B_B3	1	215	440	670	20	8.79				20*							3	195	1.00	0.33	1.03	JF
				B_B5	1									30*							5	195	1.00	0.33	1.11	JF
				B_B7	1									40*							7	195	1.00	0.33	1.17	JF
C-FRCM systems																									
[21]	CB	*1700*	1a	C1_1_R20	3	240	240	300	20	1.19	5.27	-	-	5	BD	220	4800	220.00	2.20	0.047	1	100	1.00	0.54	1.74	JF
				C1_1_R10	3	240	240	300	10												1	100	1.00	0.44	2.86	JF
				C2_1_R10	3									10							2	100	1.00	0.44	3.87	JF
				C3_1_R10	3									15							3	100	1.00	0.44	5.07	JF
				C1_1_R10	3	240	240	310	10	4.07	35.00	-	-	6	BD	270	3800	230.00	1.65	0.075	1	120	1.00	0.44	1.05	DB-JF
				C2_1_R10	3									9							2	120	1.00	0.44	1.28	DB-JF
				C3_1_R10	3									12							3	120	1.00	0.44	1.57	DB-JF
				C1_1_R20	3	240	240	310	20					6							1	120	1.00	0.54	0.87	DB-JF
				C2_1_R20	3									9							2	120	1.00	0.54	1.89	DB-JF
				C3_1_R20	3									12							3	120	1.00	0.54	2.22	DB-JF
			1b	C1_1.5_R10	3	240	360	310	10	4.76				6							1	180	1.00	0.37	1.08	DB-JF
				C2_1.5_R10	3									9							2	180	1.00	0.37	1.28	DB-JF
				C3_1.5_R10	3									12							3	180	1.00	0.37	1.55	DB-JF
			1c	C1_2_R10	3	240	480	310	10	7.38				6							1	240	1.00	0.25	0.96	DB-JF
				C2_2_R10	3									9							2	240	1.00	0.25	1.18	DB-JF
				C3_2_R10	3									12							3	240	1.00	0.25	1.23	DB-JF
[22,41]	CB	1700	4	CP_RC170_01,02	2	380	380	1000	20	12.63	6.52	-	5.90	7	BD	170	2363	220.36	1.80	0.047	2	250	1.00	0.47	1.04	JF
[40]	CB	*1700*	1a	A_CH1	1	215	215	670	20	9.97	37.80	9.30	-	10*	BD	348	4800	225.00	2.13	0.095	1	195	1.00	0.56	1.13	JF
	CB	*1700*	1a	A_CH2	1	215	215	670	20		37.80	9.30	-	15*	BD	348	4800	225.00	2.13	0.095	2	195	1.00	0.56	1.47	JF
				A_CH3	1									20*							3	195	1.00	0.56	1.61	JF
			1c	B_CH1	1	215	440	670	20	8.79				10*							1	195	1.00	0.33	1.18	JF
				B_CH2	1									15*							2	195	1.00	0.33	1.35	JF
				B_CH3	1									20*							3	195	1.00	0.33	1.37	JF
			1a	A_CL1	1	215	215	670	20	9.97				10*		220	3800	225.00	1.69	0.062	1	195	1.00	0.56	1.07	JF
				A_CL2	1									15*							2	195	1.00	0.56	1.40	JF
				A_CL3	1									20*							3	195	1.00	0.56	1.45	JF
			1c	B_CL1	1	215	440	670	20	8.79				10*							1	195	1.00	0.33	1.09	JF
				B_CL2	1									15*							2	195	1.00	0.33	1.19	JF

(*continued on next page*)

Table A1 (*continued*)

Source	Masonry			Specimens							Strengthening												Results	
											Matrix's properties				Fabric mesh's properties						Jacket					
	Type	g_m	*Scheme* [12]	*Dataset ID*	*N*	*B*	*H*	*L*	r_c	f_m	$f_{mat,c}$	$f_{mat,b}$	E_{mat}	t_{mat}	*type*	γ_f	$f_{f,u}$	E_f	$\varepsilon_{f,u}$	$t_{f,j}$	n_f	L_b	k_V	k_H	f_{mc}/f_m	FM
		[kg/m^3]			[-]	[mm]	[mm]	[mm]	[mm]	[MPa]	[MPa]	[MPa]	[GPa]	[mm]	[-]	[g/m^2]	[MPa]	[GPa]	[%]	[mm]	[-]	[mm]	[-]	[-]	[-]	
				B_CL3	1									20*							3	195	1.00	0.33	1.52	JF
G-FRCM systems																										
[37]	LS	1600	3	S_Grid	1	400	400	2100	20	4.78	13.61	5.54	-	15	BD	225	1296	72.00	1.80	0.035	1	100	1.00	0.46	1.50	DB
[41]	CB	1700	4	CP_RV320_01, 02	2	380	380	1000	20	12.63	6.52	-	5.90	7	BD	300	1200	60.00	2.00	0.064	2	250	1.00	0.47	1.07	JF
[42]	LS	1530	1a	FRCM_M4_1, 2, 3	3	250	250	500	30	7.61	4.15	-	-	10	BD	120	742.4	37.12	2.00	0.250	1	250	1.00	0.61	1.06	DB/DB-JF/S
				FRCM_M7_1, 2, 3	3						7.26	-	-	10							1	250	1.00	0.61	1.31	JF
				FRCM_M23_1, 2, 3	3	250	250	500	30		22.93	-	-	10							1	250	1.00	0.61	1.87	JF
[43]	LS	1800	1a	CM8-1, 2, 3	3	250	250	500	20	5.23	1.67	0.79	-	10	BD	220	1400	70.00	2.00	0.088	1	250	1.00	0.53	1.17	JF
	(CALC)			CM13-1, 2, 3	3						2.16	0.95	-	10							1	250	1.00	0.53	1.11	JF
				CC25-1, 2, 3	3						16.84	4.78	-	10							1	250	1.00	0.53	1.14	JF
[40]	CB	*1700*	1a	A_G3	1	215	215	670	20	9.97	37.80	9.30	-	20*	BD	220	1400	74.00	1.89	0.044	3	195	1.00	0.56	1.28	JF
				A_G5	1									30*							5	195	1.00	0.56	1.35	JF
				A_G7	1									40*							7	195	1.00	0.56	1.49	JF
			1c	B_G3	1	215	440	670	20	8.79				20*							3	195	1.00	0.33	1.02	JF
				B_G5	1									30*							5	195	1.00	0.33	1.08	JF
				B_G7	1									40*							7	195	1.00	0.33	1.12	JF
[32]	TU	1400	1a	3, 4_RM - UniSal	2	250	250	615	20	2.25	9.10	-	-	10	BD	300	1929	108.00	1.80	0.060	1	250	1.00	0.53	1.10	JF
				5, 6_RM - UniSal	2									15							2	250	1.00	0.53	1.66	JF
				7, 8_RM - UniSal	2									20							3	250	1.00	0.53	2.08	JF
	TU	1400	1a	3, 4_RM - UniPa	2	250	250	615	20	2.85	9.10	-	-	10	BD	300	1929	108.00	1.80	0.060	1	250	1.00	0.53	1.00	JF
				5, 6_RM - UniPa	2									15							2	250	1.00	0.53	1.10	JF
				7, 8_RM - UniPa	2									20							3	250	1.00	0.53	1.52	JF
	CB	1600	1a	3, 4_RM - UniCal	2	250	250	575	20	3.58	9.10	-	-	10	BD	300	1929	108.00	1.80	0.060	1	250	1.00	0.53	1.59	JF
				5, 6_RM - UniCal	2									15							2	250	1.00	0.53	2.27	JF
				7, 8_RM - UniCal	2									20							3	250	1.00	0.53	2.32	JF
	CB	1600	1a	3, 4_RM - UniNa	2	250	250	575	20	5.62	9.10	-	-	10	BD	300	1929	108.00	1.80	0.060	1	250	1.00	0.53	1.18	JF
				5, 6_RM - UniNa	2									15							2	250	1.00	0.53	1.05	JF
				7, 8_RM - UniNa	2									20							3	250	1.00	0.53	1.37	JF
PBO-FRCM systems																										
[31]	CB	*1700*	2	W_C-1, 2, 3	3	200	90	380	10	36.33	28.40	-	-	8	BD	-	5800	270.00	2.15	0.092	1	100	1.00	0.31	1.16	S
			1a	SQ_C-1, 2, 3	3	102	100	240	10	29.07											1	100	1.00	0.57	1.29	S
			1b	RECT_1_C-1, 2, 3	3	102	152	240	10	22.00											1	100	1.00	0.48	1.72	S
			1c	RECT_2_C-1, 2	2	102	204	240	10	8.90											1	100	1.00	0.35	3.97	S
[39]	CB	*1700*	1a	C-P-1	1	250	250	770	20	5.35	36.16	5.50	-	6	BD	-	3400	211.40	2.50	0.046	1	-	1.00	0.53	1.98	JF
				C-P-2	1									9							2	-	1.00	0.53	2.54	DB
				C-P-3	1									12							3	-	1.00	0.53	2.85	DB
[34]	CB	*1700*	1a	C-D-P-1L	1	250	250	770	20	5.19	36.16	5.50	-	6	BD	-	3400	211.40	2.59	0.046	1	-	0.49	0.53	1.34	DB
				C-D-P-2L	1									9							2	-	0.49	0.53	1.43	DB
				C-D-P-3L	1									12							3	-	0.49	0.53	1.93	DB
[44]	CB	*1700*	1a	LR-C1, C2, C3	3	250	250	500	30	8.52	0.79	0.64	-	10	BD	-	3300	270.00	1.49	0.014	1	300	1.00	0.61	1.21	S/DB
S-FRCM systems																										
[45]	CB	*1700*	1a	C-1-6-0-1, 2, 3, 4	4	250	250	720	0	7.38	15.00	5.00	9.00	8	UD	670	2900	205.00	2.00	0.084	1	250	1.00	0.33	1.27	DB
				C-1-6-9-1, 2, 3	3	250	250	720	9.5											0.084	1	250	1.00	0.43	1.28	DB
				C-1-6-38-1, 2, 3, 4	4	250	250	720	38.1											0.084	1	250	1.00	0.68	1.41	DB

(*continued on next page*)

Table A1 (*continued*)

B-FRCM systems																										
Source	Masonry			Specimens						Strengthening														Results		
										Matrix's properties				Fabric mesh's properties						Jacket						
	Type	g_m	*Scheme* [12]	*Dataset ID*	N	B	H	L	r_c	f_m	$f_{mat,c}$	$f_{mat,b}$	E_{mat}	t_{mat}	*type*	γ_f	$f_{f,u}$	E_f	$\varepsilon_{f,u}$	$t_{f,j}$	n_f	L_b	k_V	k_H	f_{mc}/f_m	FM
		[kg/m^3]			[-]	[mm]	[mm]	[mm]	[mm]	[MPa]	[MPa]	[MPa]	[GPa]	[mm]	[-]	[g/m^2]	[MPa]	[GPa]	[%]	[mm]	[-]	[mm]	[-]	[-]	[-]	
				C-1-12-9-1, 2, 3, 4	4	250	250	720	9.5							1200				0.169	1	250	1.00	0.43	1.35	DB
[46]	CB	*1700*	1a	C-2-6-0-1, 2, 3, 4	4	250	250	720	0	7.38	47.10	4.40	-	10	UD	670	2900	205.00	2.00	0.084	1	240	1.00	0.33	1.26	DB/JF
				C-2-6-9-1, 2, 3, 4	4	250	250	720	9.5											0.084	1	200	1.00	0.43	1.33	DB
				C-2-6-38-1, 2, 3, 4	4	250	250	720	38.1											0.084	1	200	1.00	0.68	1.39	DB/JF
				C-2-12-9-1, 2, 3, 4	4	250	250	720	9.5							1200				0.169	1	200	1.00	0.43	1.42	DB
[38]	CB	*1700*	1a	C-S-S-1, 2, 3, 4, 5	5	250	250	770	0	4.87	15.00	-	-	6	UD	670	3000	190.00	1.58	0.084	1	100	1.00	0.33	1.33	DB
[47]	CB	*1700*	1a	C-12-1-1-0	1	250	250	770	20	5.19	12.85	2.65	-	6	UD	1200	2900	205.00	2.00	0.169	1	250	1.00	0.53	2.13	DB
				C-12-2-1-0	1									9							2	250	1.00	0.53	1.96	DB
				C-12-3-1-0	1									12							3	250	1.00	0.53	2.91	DB
[39]	CB	*1700*	1a	C-S-1, 2	1	250	250	770	20	5.19	12.85	2.65	-	6	UD	1200	2900	205.00	2.00	0.169	1	250	1.00	0.53	1.82	DB
[32]	TU	1400	1a	2, 3, 4_RM - UniSa	3	250	250	615	20	3.89	13.40	-	-	10	UD	670	3080	193.40	2.17	0.084	1	375	1.00	0.53	1.12	DB
				5, 6_RM - UniSa	2									15							2	375	1.00	0.53	1.23	DB
				7, 8_RM - UniSa	2									20							3	375	1.00	0.53	1.26	DB
	TU	1400	1a	2, 3, 4_RM - UniFi	3	250	250	615	20	4.33	13.40	-	-	10	UD	670	3080	193.40	2.17	0.084	1	375	1.00	0.53	1.15	DB
				5, 6_RM - UniFi	2									15							2	375	1.00	0.53	1.28	DB
				7, 8_RM - UniFi	2									20							3	375	1.00	0.53	1.38	DB
	CB	1600	1a	2, 3, 4_RM - UniBo	3	250	250	575	20	9.09	13.40	-	-	10	UD	670	3080	193.40	2.17	0.084	1	375	1.00	0.53	2.07	DB
				5, 6_RM - UniBo	2									15							2	375	1.00	0.53	2.24	DB
				7, 8_RM - UniBo	2									20							3	375	1.00	0.53	2.52	DB
	CB	1600	1a	2, 3, 4_RM - PoliMi	3	250	250	575	20	4.92	13.40	-	-	10	UD	670	3080	193.40	2.17	0.084	1	375	1.00	0.53	1.26	DB
				5, 6_RM - PoliMi	2									15							2	375	1.00	0.53	1.33	DB
				7, 8_RM - PoliMi	1									20							3	375	1.00	0.53	1.39	DB

Legend for masonry type:
CB = clay brick.
CALC = calcarenite.
LS = limestone.
TU = tuff units.
* Assumed value.

Table A2
Experimental database organized in datasets: FRCM confined specimens with circular cross-section (8 datasets).

Source	Masonry		Specimen	Strengthening																		Results		
								Matrix's properties				Fabric mesh's properties						Jacket						
	Type	γ_m	*Dataset ID*	*N*	*D*	*L*	f_m	$f_{mat,c}$	$f_{mat,b}$	E_{mat}	t_{mat}	*type*	γ_f	$f_{f,u}$	E_f	$\varepsilon_{f,u}$	$t_{f,j}$	n_f	L_b	k_V	k_H	f_{mc}/f_m	k_e	FM
		[kg/m^3]		[mm]	[mm]	[mm]	[MPa]	[MPa]	[MPa]	[GPa]	[mm]	[-]	[g/m^2]	[MPa]	[GPa]	[%]	[mm]	[-]	[mm]	[-]	[-]	[-]	[-]	
[48]	LS *(CALC)*	2000	BG.01.01, 02, 03, 04	4	83	218	20.79	28.00	10.00	11.00	7	BD	250	1542	89.00	1.80	0.039	1	130	1.00	1.00	1.21	0.11	JF
			BG.03.01, 02, 03, 04	4							10							3	130	1.00	1.00	1.24	0.23	JF
[49]	CB	*1700*	C1, 2, 3, 4M_W1L	4	94	190	25.19	25.00	8.00	10.00	4	BD	250	1542	89.00	1.80	0.039	1	100	1.00	1.00	1.27	-	JF
			C1, 2, 3M_W2L	3							6							2	100	1.00	1.00	1.38	-	JF
			C1, 2, 3M_C1L	3			19.85				4							1	100	1.00	1.00	1.66	-	JF
			C1, 2M_C2L	2							6							2	100	1.00	1.00	1.85	-	JF
G-FRCM systems																								
[48]	LS	2000	GG.01.01, 02, 03, 04	4	83	218	20.79	28.00	10.00	11.00	7	BD	125	1276	72.00	1.80	0.024	1	130	1.00	1.00	1.01	0.22	JF
	(CALC)		GG.03.01, 02, 03, 04	4							10							3	130	1.00	1.00	1.26	0.20	JF

Legend for masonry type:
CALC = calcarenite.
CB = clay brick.
LS = limestone.

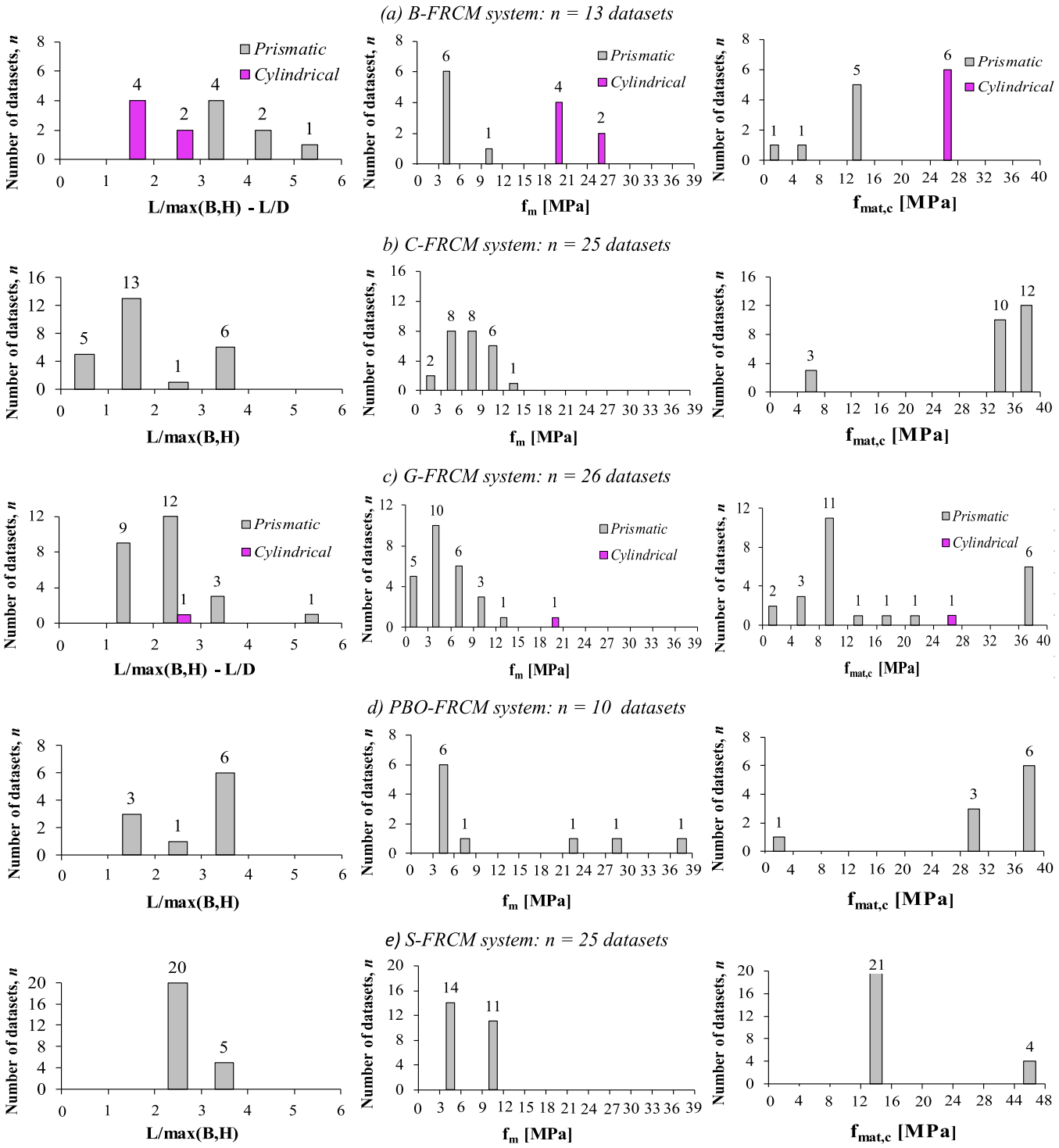

Fig. A1. Values and corresponding number of datasets used in the analyses of three main parameters.

1) the ratio of the column length to the major side dimension of the cross section $L/\max(B,H)$, which is replaced by L/D in the case of members with circular section;
2) the compressive strength of unconfined masonry, f_m;
3) the compressive strength of the inorganic matrix, $f_{mat,c}$.

Focusing on the 13 datasets related to tests performed on masonry columns confined with B-FRCM system (Fig. A.1a), the following main considerations are made:

1. for what concern the geometry, the datasets related to prismatic specimens are quite homogeneous. Indeed, these specimens have always square cross-section with the parameter $L/\max(B,H)$ ranging between 1 and 3. In the case of the cylindrical specimens a slightly greater variation is observed for the values assumed by the L/D ratio;
2. the most scattered values are found for the compressive strength of the unconfined masonry f_m, ranging between 4.7 (see range 3–6 MPa for prismatic specimens) and 25.2 MPa (see range 24–27 MPa for cylindrical specimens), and, even more, for the compressive strength of the inorganic matrix $f_{mat,c}$, ranging between 0.6 (see range 0–4 MPa for prismatic specimens) and 28 MPa (see range 24–28 MPa for cylindrical specimens).

Focusing on the 25 datasets related to tests performed on specimens confined with C-FRCM system (Fig. A1b), the following considerations are made:

1. for what concern the geometry, 11 datasets entail prismatic columns having rectangular section with side ratio equal to 1.5 (#3 datasets) or 2 (#8). The parameter $L/\max(B,H)$ is quite scattered, with values spanning between 0.6 and 3.1 and highest concentration in the range 1–2 (#13 datasets);
2. the range of f_m values experimentally investigated is narrower than that found for masonry samples confined with B-FRCM system, with the highest frequency in the ranges 3–6 and 6–9 MPa. Similarly, the values of $f_{mat,c}$ are concentrated within few ranges, even though for 3 datasets $f_{mat,c}$ is about 6 MPa (rather low value, see range 4–8 MPa) and for 22 datasets is in the range 32–40 MPa;

Focusing on the 26 datasets related to test performed on columns confined with G-FRCM system (Fig. A1c), the following considerations can be drawn:

1. for what concern the geometry, 22 out of 26 datasets related to prismatic specimens are squared, and the parameter $L/\max(B,H)$ is mostly concentrated in the ranges 1–2 and 2–3;
2. a wide range of f_m values was experimentally investigated, spanning between 2.3 and 20.8 MPa; the highest concentration of values is in the range 3–6 (#10 datasets). Also, the parameter $f_{mat,c}$ is quite scattered; the most frequently used value was $f_{mat,c} = 9.1$ MPa, included in the range 8–12 MPa ($n = 11$), even though 6 datasets entail specimens with medium–high strength inorganic matrices ($f_{mat,c} = 37.8$ MPa, see range 36–40 MPa);

Focusing on the 10 datasets related to test performed on columns confined with PBO-FRCM system (Fig. A1d), the following observations can be made:

1. for what concern the geometry, 8 out of 10 datasets entail square specimens ($n = 8$); the parameter $L/\max(B,H)$ is only slightly scattered, and 3.1 is the mostly investigated value ($n = 6$, see the range 3–4);
2. the f_m values are mostly concentrated in the range 3–6 MPa ($n = 6$), but they span from 5.2 to 36.3 MPa; conversely, the compressive strength of the inorganic matrix is mostly uniform.

Finally, focusing on the 25 datasets related to test performed on samples confined with S-FRCM system (Fig. A1e), the following main considerations are made:

1. for what concern the geometry, all datasets entail square specimens with ratios L/B rather homogeneous in the range 2–3 and 3–4;
2. the investigated specimens are characterized by f_m values spanning between 3.9 (see range 3–6 MPa, $n = 14$) and 9.1 MPa (see range 9–12 MPa, $n = 11$), with the highest concentration about 9.1 MPa. For what concerns the inorganic matrix, the highest concentration is in the range 12–16 MPa ($n = 21$) even though 4 datasets include specimens with $f_{mat,c}$ values equal to 47.1 MPa.

References

[1] Ekenel M, De Caso y Basalo FJ, Nanni N. Acceptance Criteria for Concrete and Masonry Strengthening Using Fabric-Reinforced Cementitious Matrix (FRCM) and Steel Reinforced Grout (SRG) Composites. ACI SP-324-04; 2018.

[2] AC434. ICC-ES Acceptance Criteria for Masonry and Concrete Strengthening Using Fiber-reinforced Cementitious Matrix (FRCM) and Steel Reinforced Grout (SRG) Composite Systems. AC434, ICC Evaluation Services, Inc., Los Angeles, CA. June 2016.

[3] Yan LB, Chouw N, Jayaraman K. Flax fibre and its composites—A review. Compos Part B 2014;56:296–317.

[4] Dittenber DB, GangaRao HVS. Critical review of recent publications on use of natural composites in infrastructure. Compos Part A 2012;43:1419–29.

[5] Cevallos OA, Olivito R, Codispoti R. Experimental Analysis of Repaired Masonry Elements with Flax-FRCM and PBO-FRCM Composites Subjected to Axial Bending Loads. Fibers 2015;3:491–503.

[6] Mercedes L, Bernat-Maso E, Gil L. In-plane cyclic loading of masonry walls strengthened by vegetal-fabric reinforced cementitious matrix (FRCM) composites. Eng Struct 2021;221:111097.

[7] Banholzer B, Brockmann T, Brameshuber W. Material and bonding characteristics for dimensioning and modeling of textile reinforced concrete (TRC) elements. Mater Struct 2006;39:749–63.

[8] Triantafillou TC, Papanicolaou CG. Shear strengthening of reinforced concrete members with textile reinforced mortar (TRM) jackets. Mater Struct 2006;39:93–103.

[9] Ascione L, de Felice G, De Santis S. A qualification method for externally bonded Fiber Reinforced Cementitious Matrix (FRCM) strengthening systems. Compos Part B 2015:497–506.

[10] Tetta ZC, Triantafillou TC, Bournas DA. On the design of shear-strengthened RC members through the use of textile reinforced mortar overlays. Compos Part B 2018;147:178–96.

[11] ICOMOS/Iscarsah Committee 2005. Recommendations for the analysis, conservation and structural restoration of architectural heritage. Accessed June 15, 2021. http://www.icomos.org.

[12] Al-Jaberi Z, Myers JJ, Gawad M. Pseudo-static cyclic loading comparison of reinforced masonry walls strengthened with FRCM or NSM FRP. Constr Build Mater 2018;167:482–95.

[13] Wang X, Lam CC. Comparison of different types of TRM composites for strengthening masonry panels. Constr Build Mater 2019;219:184–94.

[14] Angiolilli M, Gregori A, Pathirage M, Cusatis G. Fiber Reinforced Cementitious Matrix (FRCM) for strengthening historical stone masonry structures: Experiments and computations. Eng Struct 2020;224:111102.

[15] Scacco J, Ghiassi B, Milani G, Lourenço PB. A fast modeling approach for numerical analysis of unreinforced and FRCM reinforced masonry walls under out-of-plane loading. Compos B Eng 2020;180:107553.

[16] Donnini J, Maracchini G, Lenci S, Corinaldesi V, Quagliarini E. TRM reinforced tuff and fired clay brick masonry: Experimental and analytical investigation on their in-plane and out-of-plane behavior. Constr Build Mater 2021;272:121643.

[17] Castellano A, Fraddosio A, Oliveira DV, Piccioni MD, Ricci E, Sacco E. An effective numerical modelling strategy for FRCM strengthened curved masonry structures. Eng Struct 2023;274:115116.

[18] Alecci V, Focacci F, Rovero L, Stipo G, De Stefano M. Intrados strengthening of brick masonry arches with different FRCM composites: Experimental and analytical investigations. Compos Struct 2017;176:898–909.

[19] Napoli A, Realfonzo R. Compressive Behavior of Masonry Columns Confined with FRCM Systems: Research Overview and Analytical Proposals. J Compos Constr 2022;26(3):04022019.

[20] Carloni C, Mazzotti C, Savoia M, Subramaniam KV. Confinement of masonry columns with PBO FRCM composites. Key Eng Mater 2015;624:644–51.
[21] Krevaikas, T. Textile Reinforced Mortar System as a means for confinement of masonry structures. In: Proc., 12th Int. Symposium on Fiber Reinforced Polymers for Reinforced Concrete Structures (FRPRCS-12) and 5th Asia-Pacific Conference on Fiber Reinforced Polymers in Structures (APFIS-2015), Nanjing. China, 2015.
[22] Incerti A, Vasiliu A, Ferracuti B, Mazzotti C. Uni-axial Compressive tests on masonry columns confined by FRP and FRCM. In: Proc., 12th Int. Symposium on Fiber Reinforced Polymers for Reinforced Concrete Structures (FRPRCS-12) and 5th Asia-Pacific Conference on Fiber Reinforced Polymers in Structures (APFIS-2015), Nanjing. China, 2015.
[23] Kouris LAS, Triantafillou TC. State-of-the-art on strengthening of masonry structures with textile reinforced mortar (TRM). Constr Build Mater 2018;188:1221–33.
[24] Irandegani MA, Zhang D, Shadabfar M, Kontoni D-P-N, Iqbal M. Failure Modes of RC Structural Elements and Masonry Members Retrofitted with Fabric-Reinforced Cementitious Matrix (FRCM) System: A Review. Buildings 2022;12:653.
[25] de Felice G, De Santis S, Realfonzo R, Napoli A, Ascione F, Stievanin E, et al. State of the art of steel reinforced grout applications to strengthen masonry structures. ACI Special Publication (SP 326) 2018. 102.1-102.12.
[26] Krzywoń R. Steel-Reinforced Polymers and Steel-Reinforced Composite Mortars for Structural Applications—An Overview. J Compos Sci 2020;4(3):142.
[27] De Santis S, Ceroni F, de Felice G, Fagone M, Ghiassi B, Kwiecień A, et al. Round Robin Test on tensile and bond behaviour of Steel Reinforced Grout systems. Compos B Eng 2017;127:1–120.
[28] de Felice G, Aiello MA, Caggegi C, Ceroni F, De Santis S, Garbin E, et al. Recommendation of RILEM Technical Committee 250-CSM: Test method for Textile Reinforced Mortar to substrate bond characterization. Mater Struct 2018;51:95.
[29] National Research Council (CNR). Guide for the design and construction of externally bonded fibre reinforced inorganic matrix systems for strengthening existing structures. CNR-DT 215/2018. Rome, Italy (version of June 30, 2020).
[30] American Concrete Institute (ACI). Guide to Design and Construction of Externally Bonded Fabric-Reinforced Cementitious Matrix (FRCM) and Steel-Reinforced Grout (SRG) Systems for Repair and Strengthening Masonry Structures. ACI 549.6R 2020, Farmington Hills, MI.
[31] Carloni C, Mazzotti C, Savoia M, Subramaniam KV. Confinement of Masonry Columns with PBO FRCM Composites. Key Eng Mater 2018;624:644–51.
[32] Aiello MA, Bencardino F, Cascardi A, D'Antino T, Fagone M, Frana I, et al. Masonry columns confined with fabric reinforced cementitious matrix systems: A round robin test. Constr Build Mater. 2021, 298, 1-31. Article number: 123816.
[33] Napoli A, Realfonzo R. FRP confined masonry under compression: database collection and design proposals. Compos Struct 2021;276(1–24):114490.
[34] Aiello MA, Cascardi A, Ombres L, Verre S. Confinement of Masonry Columns with the FRCM-System: Theoretical and Experimental Investigation. Infrastructures 2020;5:101.
[35] Fossetti M, Minafò G. Strengthening of masonry columns with BFRCM or with steel wires: an experimental study. Fibers 2016;4(15):1–10.
[36] Mezrea PE, Ispir M, Binbir E, Bal IE, Ilki A. External jacketing of unreinforced historical masonry piers with open-grid basalt-reinforced mortar. J Compos Constr 2017;21(3):1–16.
[37] Maddaloni G, Cascardi A, Balsamo A, Di Ludovico M, Micelli F, Aiello MA, et al. Confinement of Full-Scale Masonry Columns with FRCM Systems. Key Eng Mater 2017;747:374–81.
[38] Santandrea M, Quartarone G, Carloni C, Gu X. Confinement of Masonry Columns with Steel and Basalt FRCM Composites. Key Eng Mater 2017;747:644–51.
[39] Ombres L, Iorfida A, Verre S. Confinement of Masonry Columns with PBO and Basalt FRCM Composites. Key Eng Mater 2019;817:392–7.
[40] Koutas LN, Bournas DA. Confinement of masonry columns with textile-reinforced mortar jackets. Constr Build Mater 2020;258. 120343.
[41] Murgo FS, Mazzotti C. Masonry columns strengthened with FRCM system: Numerical and experimental evaluation. Constr Build Mater 2019;202:208–22.
[42] Cascardi A, Micelli F, Aiello MA. FRCM-confined masonry columns: experimental investigation on the effect of the inorganic matrix properties. Constr Build Mater 2018;2018(186):811–25.
[43] Minafò G, La Mendola L. Experimental investigation on the effect of mortar grade on the compressive behaviour of FRCM confined masonry columns. Compos B Eng 2018;146:1–12.
[44] Alecci V, De Stefano M, Galassi S, Magos R, Stipo G. Confinement of Masonry Columns with Natural Lime-Based Mortar Composite: An Experimental Investigation. Sustainability 2021;13:13742.
[45] Sneed LH, Carloni C, Baietti G, Fraioli G. Confinement of clay masonry columns with SRG. Key Eng Mater 2017;747:350–7.
[46] Sneed LH, Baietti G, Fraioli G, Carloni C. Compressive Behavior of Brick Masonry Columns Confined with Steel-Reinforced Grout Jackets. J Compos Constr 2019;23(5):04019037.
[47] Ombres L, Verre S. Masonry columns strengthened with Steel Fabric Reinforced Cementitious Matrix (S-FRCM) jackets: Experimental and numerical analysis. Measurement 2018;127:238–45.
[48] Estevan L, Baeza FJ, Bru D, Ivorra S. Stone masonry confinement with FRP and FRCM composites. Constr Build Mater 2020;237:1–12.
[49] D'Anna J, Amato G, Chen JF, Minafò G, La Mendola L. Experimental investigation on BFRCM confinement of masonry cylinders and comparison with BFRP system. Constr Build Mater 2021;297:123671.
[50] Realfonzo R, Napoli A. Confining concrete members with FRP systems: Predictive vs design strain models. Compos Struct 2013;104:304–19.
[51] Napoli A, Realfonzo R. Compressive behavior of concrete confined by SRP wraps. Constr Build Mater 2016;127:993–1008.
[52] Faella C, Napoli A, Realfonzo R. Confinement of concrete with FRCM materials. Lecture Notes in Civil Engineering 2020;42:360–71.
[53] Napoli A, Realfonzo R. Compressive strength of concrete confined with fabric reinforced cementitious matrix (FRCM): Analytical models. JCOMC 2020, 2, 1-22. Article number 100032; 2020.
[54] CEN, European Committee for Standardization. (2002). EN 1990:2002. Eurocode 0: Basis of structural design.
[55] National Research Council (CNR). Guide for the design and construction of externally bonded FRP systems for strengthening existing structures. CNR-DT200 R1, Rome, Italy.
[56] Faella C, Martinelli E, Camorani G, Aiello MA, Micelli F, Nigro E. Masonry columns confined by composite materials: Design formulae. Compos B Eng 2011;42(4):705–16.
[57] Napoli A, Realfonzo R. Compressive strength of masonry confined by FRCM systems: Assessment of existing models and new proposals. In: Proc., XIX ANIDIS Conference, Seismic Engineering in Italy, Turin, 11-15 September 2022.
[58] American Concrete Institute (ACI). Guide for the Design and Construction of Externally Bonded FRP Systems for Strengthening Concrete Structures. ACI 440.2R 2017, Farmington Hills, MI: ACI.